ANL-HEP-CP--93-01

DE93 006412

ANL-HEP-CP-93-01
For the Proceedings of the
RCNP Kikuchi School on
Spin Physics at Intermediate Energies
Osaka, Japan
16-19 November 1992

OVERVIEW OF SPIN PHYSICS*

A. Yokosawa

High Energy Physics Division
Argonne National Laboratory, Argonne, Illinois 60439 USA

23 December 1992

Abstract

We review spin-physics experiments carried out during the past roughly thirty years, significant physics accomplished, and future prospects.

CONTENTS

Spin physics activities at medium and high energies became significantly active when polarized targets and polarized beams became accessible for hadron-hadron scattering experiments. My overview of spin physics will be inclined to the study of strong interaction using facilities at Argonne ZGS, Brookhaven AGS (including RHIC), CERN, Fermilab, LAMPF, and SATURNE. General references for the first two sections are Refs. 1 to 5.

In 1960 accelerator physicists had already been convinced that the ZGS could be unique in accelerating a polarized beam; polarized beams were being accelerated through linear accelerators elsewhere at that time.

However, there was much concern about going ahead with the construction of a polarized beam because i) the source intensity was not high enough to accelerate in the accelerator, ii) the use of the accelerator would be limited to only polarized-beam physics, that is, proton-proton interaction, and iii) p-p elastic scattering was not the most popular topic in high-energy physics.

In fact, within spin physics, π-nucleon physics looked attractive, since the determination of spin and parity of possible πp resonances attracted much attention. To proceed we needed more data beside total cross sections and elastic differential cross sections; measurements of polarization and other parameters were urgently needed.

Polarization measurements had traditionally been performed by analyzing the spin of recoil protons. The drawbacks of this technique are: i) it involves double scattering, resulting in poor accuracy of the data, and ii) a carbon analyzer can only be used for a limited region of energy.

1. Experiments with Polarized Targets

In 1961, solid-state physicists at Berkeley, Harvard, and Saclay had succeeded in polarizing protons in a crystal. High-energy physicists at Berkeley, Rutherford, CERN, Argonne, and Saclay had begun planning to make use of a polarized proton target.

The main advantage of the use of a polarized target is that one can measure polarization by single scattering. But the only material available in 1962 was a crystal lanthanam magnesium nitrate, $La_2Mg_3(NO_3) \cdot 24\ H_2O$). We had to be convinced that we could carry out πp elastic scattering measurements using such a crystal at π incident momentum as high as 10 GeV/c; counting on the Fermi-momenta spread due to bound protons, we could select events that occurred only with free protons that are polarized.

Experiments using polarized targets were first concentrated in clarifying the spin and parity of πp resonances by measuring $\pi p^{\uparrow} \rightarrow \pi p$ at various angles covering these energy regions up to 3 GeV/c where bumps were shown in πp total cross sections. These attempts were successful in establishing various resonance states.

In 1966, the energy regions beyond resonances were investigated. We found mirror symmetry in the π^+p and π^-p world as shown in Fig. 1. Measurements in $\pi^- p^{\uparrow} \rightarrow \pi^0 n$ were also performed and the results of non-zero asymmetry destroyed a "naive" Regge-pole model which was popular at the time.

In 1968, there was a new break through with the invention of new hydrocarbon target (cleaner material than the crystal) at ^{3}He temperature yielding 80% of polarization. The new target greatly promoted spin physics activities. We show some theorists appreciation of polarized targets comically expressed in Fig. 2.

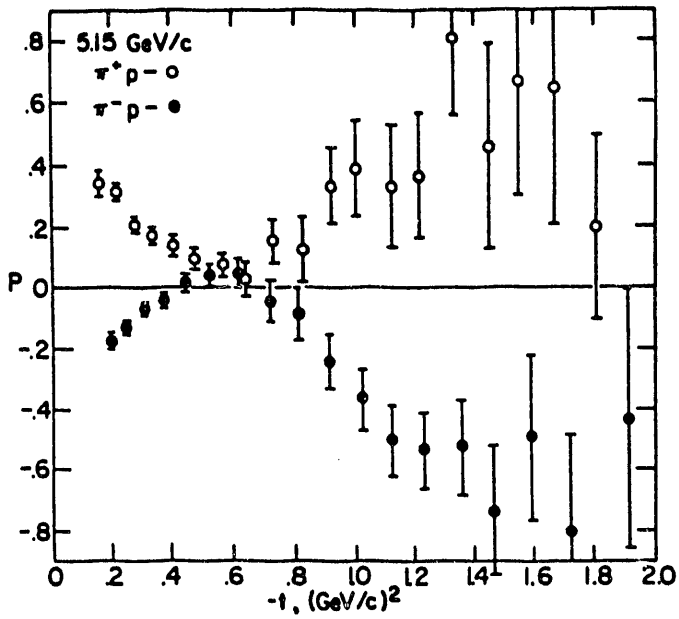

Figure 1. Polarization of $\pi^{\pm}$ elastic scattering.

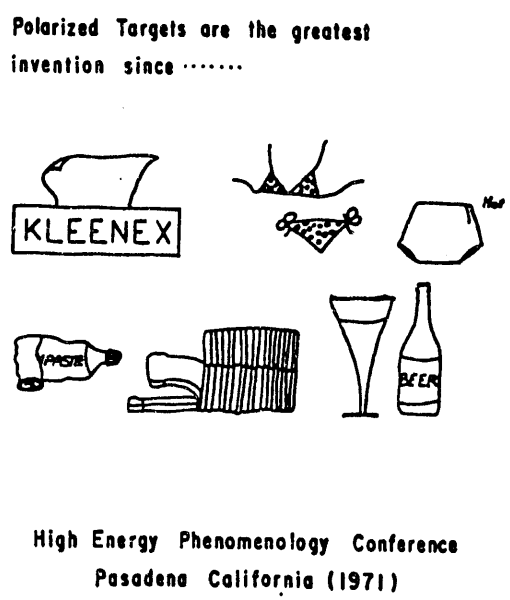

Figure 2. Appreciation from theorists.

2. Experiments with Polarized Beams and Polarized Targets (Medium Energies)

In 1973, polarized protons were accelerated to 6 GeV/c and later above 11 GeV/c at the ZGS. Also later polarized beams became available at KEK, AGS, LAMPF, and Saturne. Then the major concentration on spin physics was shifted to pp scattering in which two-spin and three-spin measurements could be done.

Let us list some observables in the pp interactions. We adopt the notation (Beam, Target; Scattered, Recoil or X) to express the observables; * indicates that the spin direction is known; O means that the spin direction is not known. N is normal to the scattering, while L is the longitudinal direction, and S is NxL in the scattering plane.

Observables	Description	Symbol
(O,O;O,O)	Cross Section	σ
(*,O;O,O) or (O,*;O,O)	Analyzing Power (polarization parameter)	A_N (P)
(*,*;O,O)	Spin-Spin Correlation	A_{LL} (C_{LL}), A_{NN} (C_{NN}), A_{SS} (C_{SS})
(*,O;O,*)	Polarization Transfer	K_{ik}
(O,*;O,*)	Depolarization Parameter	D_{ik}
(*,*;O,*)	Triple-Spin Parameter	H_{ijk}

For example, to determine the parameter A_N, one measures the difference between the number of events with spin up and down divided by the sum; that is

$$A_N = (1/P_B)\,(N^{\uparrow} - N^{\downarrow})/((N^{\uparrow} + N^{\downarrow}).$$

To determine the correlation parameter A_{NN}, one measures the difference between the event rate with parallel and antiparallel spin directions divided by the sum, and the result then divided by the product of the beam (P_B) and target (P_T) polarizations:

$$A_{NN} = \frac{1}{P_B P_T} (N^{\uparrow\uparrow} + N^{\downarrow\downarrow} - N^{\uparrow\downarrow} - N^{\downarrow\uparrow})/(N^{\uparrow\uparrow} + N^{\downarrow\downarrow} + N^{\uparrow\downarrow} + N^{\downarrow\uparrow}).$$

The correlation parameter A_{LL} is expressed as:

$$A_{LL} = \frac{1}{P_B P_T} (I^{++} - I^{+-})/(I^{++} + I^{+-}) = \frac{1}{P_{BT}} (N^{\rightleftarrows} - N^{\rightrightarrows})/(N^{\rightleftarrows} + N^{\rightrightarrows}),$$

where (++) refers to the spin state parallel-equal helicity and (+-) to the spin state antiparallel-opposite helicity in the c.m. system. Since the incident hadrons have opposite momenta in the c.m. of the interactions, I^{++} (I^{+-}) events are measured in antiparallel, $N^{\rightleftarrows}$, (parallel, $N^{\rightrightarrows}$) spin states of the beam and target particles.

The spin-dependent total cross sections are:

$$\Delta\sigma_L = [\sigma^{Tot}(\rightleftarrows) - \sigma^{Tot}(\rightrightarrows)] \text{ (longitudinal spins) and}$$

$$\Delta\sigma_T = [\sigma^{Tot}(\uparrow\downarrow) - \sigma^{Tot}(\uparrow\uparrow)] \text{ (transverse spins) ,where}$$

$$\sigma^{Tot} = 1/2[\sigma^{Tot}(\rightleftarrows) + \sigma^{Tot}(\rightrightarrows)].$$

In 1976, there was a big surprise in spin physics. Experiments carried out to measure $\Delta\sigma_L(pp)$ found a sizable structure in the pp system. As shown in Fig. 3, up to 1.2-GeV/c incident

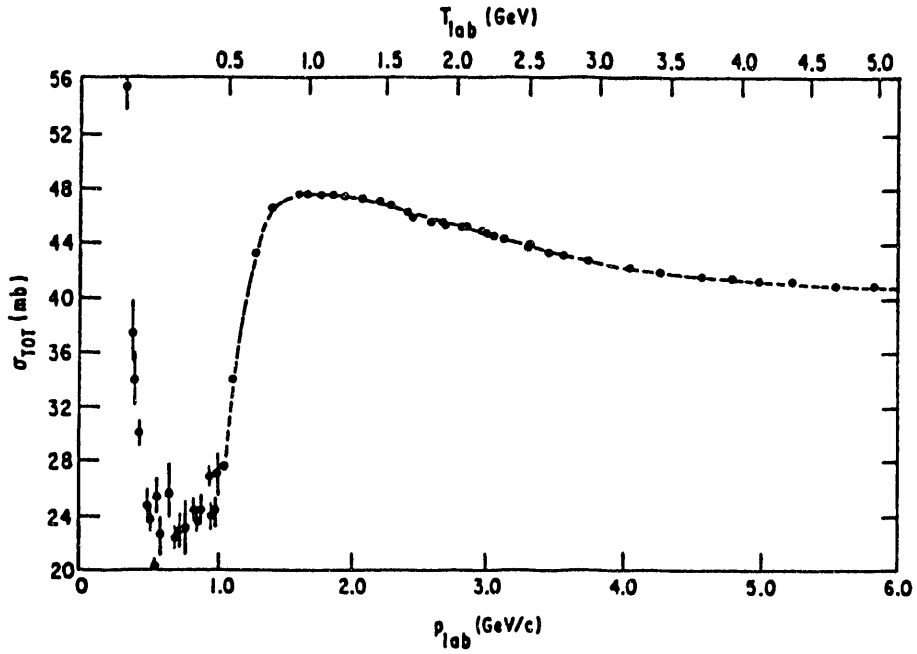

Figure 3. pp total cross section.

proton momentum, the total cross section, which mainly consists of the elastic process, falls and then rises due to opening of the inelastic-channel. The cross section flattens above 1.5 GeV/c. We observe no structures in the total cross section. As shown in Fig. 4, the $\Delta\sigma_L$ data show a sharp peak near 1.2 GeV/c and a dip near 1.5 GeV/c.

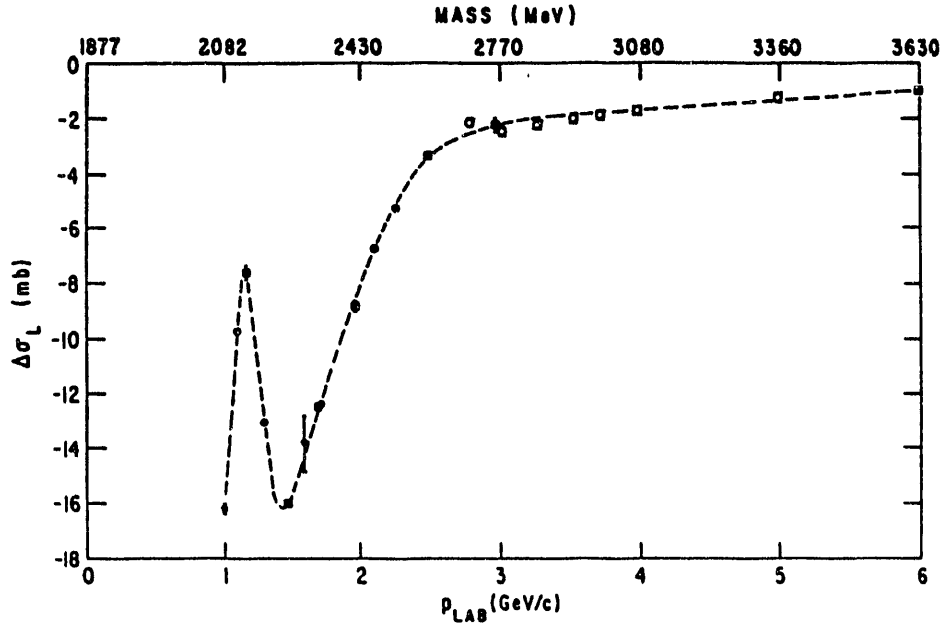

Figure 4. Difference in the total cross section, $\Delta\sigma_L$.

To understand this phenomena, during the following several years, many observables mentioned above were measured in the pp system at several laboratories. These results were indispensable in obtaining unique partial-wave solutions. Two dibaryon resonances, $^1D_2$ and $^3F_3$, in the I = 1 system were found. At present, studies in the np system are continuing and there is a good dibaryon candidate in the I = 0 system as shown in Fig. 5.[6]

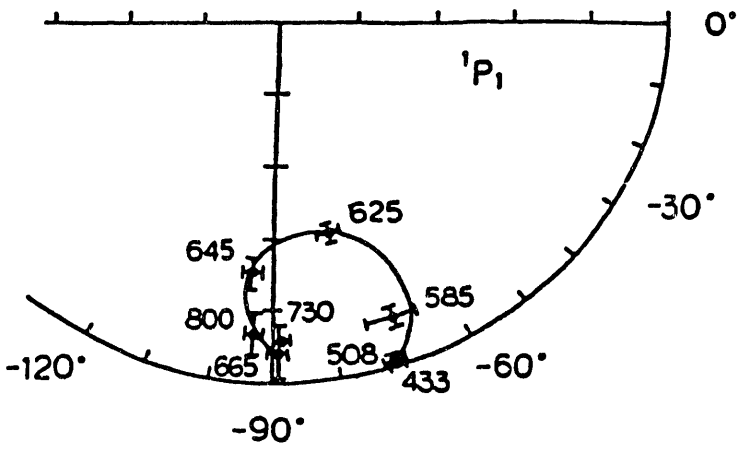

Figure 5. I=0 dibaryon candidate.

There was confusion once when a partial wave analysis for $NN \rightarrow NN\pi$ reaction was interpreted that there was no evidence for the existence of the $^1D_2$ dibaryon.[7] Recently it was found that the interpretation was not appropriate because there are two important effects on the phases for $pp \rightarrow np\pi^+$ not taken into account. Now the $N\Delta$ phase in the $NN \rightarrow NN\pi$ partial-wave analysis can be explained on the basis of the S-matrix pole for the $^1D_2$-wave pp, $^5S_2$-wave $N\Delta$, and $^3P_2$-wave πd scattering.[8] The details are shown in Fig. 6.

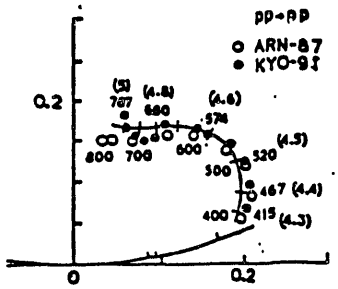

Argand plots for $pp(^1D_2)-pp(^1D_2)$. Numbers are T_{lab} (s) in MeV(GeV^2).

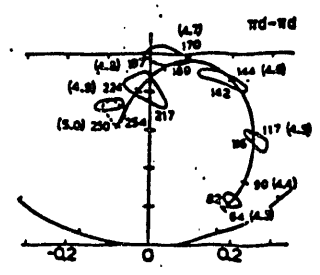

Argand plots for $\pi d(^3P_2)-\pi d(^3P_2)$. Numbers are T_{lab} (s) in MeV(GeV^2). The regions drawn for each energy are the PWA results.

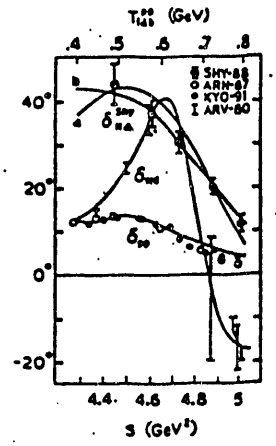

Plots of $\delta_{N\Delta}^{SHY}(^5S_2)$, $\delta_{pp}(^1D_2)$ and $\delta_{\pi d}(^3P_2)$ vs. s. Solid curves are our prediction. PWA results of SHY-88, ARN-87 and KYO-91 are given in comparison.

Figure 6. Consistency check for dibaryon.

To further understand these effects, one must look for structures in energy much higher than the threshold region. Results at p_{lab} = 2 to 6, and 11.75 GeV/c are shown in Fig. 7 revealing bump and dip structures in the momentum range 2.5 to 4.0 GeV/c. If the bumps in $(k^2/4\pi)\,\Delta\sigma_L$ are considered to be due to diproton resonances, the masses are about 2700 and 2900 MeV.

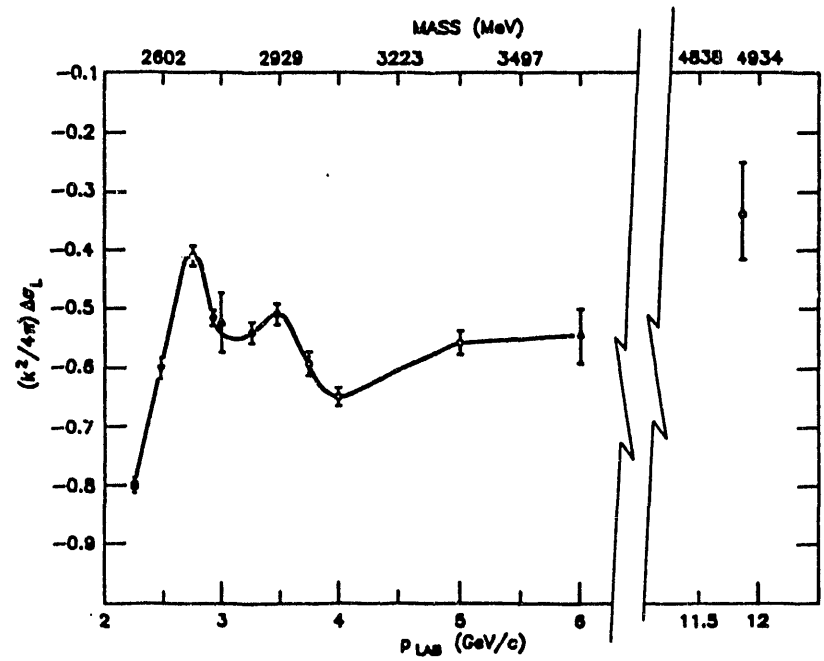

Figure 7. A plot of $(k^2/4\pi)\,\Delta\sigma_L$ vs. mass. The line drawn is only to guide the eye.

2.1 Candidates for Dibaryon Resonances

We summarize candidates for I = 0 and I = 1 dibaryon resonances in the nucleon-nucleon system in Table 1. (The I = 0 isospin state has fewer candidates than I = 1 because of the lack of experimental data.)

Table I. Candidates for the Dinucleon Resonances

(i) I = 1 Isospin State							
	B_1^2 2.14	B_1^2 (2.18)	B_1^2 (2.22)	B_1^2 (2.43)	B_1^2 (2.43)	B_1^2 (2.70)	B_1^2 (2.90)
T(MeV)	564	656	750	1,270	1,270	2,008	2,605
Mass, GeV	2.14-2.17	2.18-2.20	2.20-2.25	2.43-2.50	2.43-2.50	2.70 ± 0.10	2.90 ± 0.10
Width, GeV	50-100	100-200	100-200	~ 150	~ 150	~ 150	~ 150
Quantum State	$^1D_2$	Triplet P	$^3F_3$	Probably $^1G_4$	Triplet R_{JJ}		Probably $^1I_6$
	pp (10%)	pp (10%)	pp (17%)				
Decay Modes	πd (30%)	πd (30%)	πd (4%)				
	NΔ (35%)						

(ii) I = 0 Isospin State		
	B_0^2 (2.17)	B_0^2 (2.43)
T (MeV)	750	1,270
Mass, GeV	2.17	2.40 - 2.50
Width, MeV	25	~ 200
Quantum State	$^1P_1$	Triplet

The current status of non-strange dibaryon resonances in the region of masses 1.88 - 3.02 GeV was reviewed by I. Strakovsky[9] by examining $NN \rightarrow NN$, $\pi d \rightarrow \pi d$, $NN \rightarrow \pi d$, $NN \rightarrow \Delta N$ channels. A similar conclusion was drawn as those in Table 1. It was concluded that a combined analysis in the framework of coupled channels should bring us to the clarification of dibaryon resonances.

2.2 A Study of N-N Spin Observables at Saturne

A number of measurements are being and will be made to study pp and np elastic scattering and total cross section spin observables in the beam kinetic-energy range from 0.5 to 2.7 GeV at Saturne. The goals will include i) a determination of the I = 0 amplitudes to higher energies, and ii) the identification of the partial wave(s) responsible for structure previously observed at Saturne II and Argonne ZGS energies.

Measurements of the I = 0 amplitudes above 1.1 GeV from quasielastic scattering of a polarized proton beam from a polarized deuterium target will be performed. The measurements will be performed detecting the outgoing neutron and proton in coincidence.

The numerous indications of structure in the cross sections and spin observables near $T_{lab} \approx 2100$ MeV require additional measurements to their origin. This energy is higher than that covered by most phase-shift analyses.

2.3 πd and pd Elastic Scattering

Results of cross section, tensor polarization, and vector polarization measurements in πd elastic scattering of PSI, LAMPF, TRIUMF, and KEK energies have been reviewed earlier (for instance, Ref. 4). For the tensor polarization t_{20}, there exist two different data sets which differ dramatically. The measurements were performed at LAMPF[10] and the other at PSI.[11] The LAMPF data show that the angular distribution of t_{20} is negative and smooth. The PSI data, on the other hand, show a positive and rapid angular dependence. Relatively new data from TRIUMF[12,13] are in agreement with the LAMPF data.

A phenomenological analysis of pion-deuteron elastic scattering was carried out[14] by using a model that contains the dibaryon resonance amplitude and the background amplitude obtained by a Glauber-model calculation.[15] The experimental data used in the analysis include differential cross section, the vector analyzing power, and the tensor polarization in the momentum region 250 to 1000 MeV/c. No satisfactory fit to the t_{20} PSI data[11] with the rapid angular dependence was found, but it is important to note that resonance parameters were needed for satisfactory fits. In this energy region, it is practically impossible to perform a phase-shift analysis because of the large number of partial waves required. Therefore, the above model, which gives the non-resonance amplitudes without any serious ambiguity, was used to interpret the existing data.

The analyzing power for elastic pd scattering ($p^{\uparrow}d \rightarrow pd$) has been measured in the forward region at 800 MeV and at 3.5 GeV (Refs. 16 and 17, respectively). These angular distributions show that the behavior is consistent with the prediction of the multiple scattering model based on the Glauber theory.

Various spin parameters for $p^{\uparrow}d \rightarrow p^{\uparrow}d$ scattering were measured at 496, 647, and 800 MeV.[18] Comparison with the noneikonal multiple scattering theory[19] reveals large discrepancies between the data and theory at 800 and 650 MeV but fairly good agreement at 500 MeV. Spin observables in small-angle elastic $p^{\uparrow}d \rightarrow p^{\uparrow}d$ scattering were measured with an N-type target[20] and an L-type magnet[21] at 800 MeV. The results were compared with predictions based on different phase-shift solutions for the nucleon-nucleon scattering matrix.

A number of vector and tensor spin observables in the d-p elastic scattering reaction were measured at Saturne II[22] with a polarized deuteron beam at incident energy of 1.6 GeV.

2.4 $pp \rightarrow \pi d$ Scattering

Earlier extensive $\pi d^+ \rightarrow pp$ phase-shift analyses were performed.[23] The results show good agreement with the various experimental data.[24-26] The phase-shift results include the Breit-Wigner behavior for $J^P = 2^+$ and 3^- ($^1D_2$ and $^3F_3$) states. A similar result was obtained by a $\pi d \rightarrow \pi d$ phase-shift analysis.[27]

It is important to note that the $\pi^+d \rightarrow pp$ phase shifts[23] give M ~ 2.17 GeV and Γ_{tot} ~ 0.11 GeV for NN states $^1D_2$, $^3F_3$, and $^3P_1$. Similar results were obtained by K-matrix analysis of pp scattering at $\sqrt{s}$ = 1.88 - 2.36 GeV for NN states $^1D_2$, $^3F_3$, and $^3P_2$ - $^3F_2$ partial waves.[28] Also, K-matrix analysis for systems pp, NΔ, and πd at $\sqrt{s}$ = 2.02 - 2.34 GeV gave M ~ 2.16 GeV for $^1D_2$ and $^3F_3$ states.[29] Slightly different results from the above analyses were reported.[30]

Spin-spin correlation parameters (A_{LL} and A_{SL}) for $p^{\uparrow}p^{\uparrow} \rightarrow \pi d$ were measured between 500 and 800 MeV at LAMPF.[31,32] The results are consistent with predictions of PWA from Ref. 29, but they are in substantial disagreement with theoretical predictions[33] above 600 MeV.

All non contradictory πd elastic and $\pi^+d \rightarrow pp$ PWAs yield a branching ratio of $\Gamma_{\pi d}/\Gamma_{Tot}$ ~ 0.3 (Γ_{pp}/Γ_{tot} ~ 0.1) for both the $^1D_2$ and P wave NN states in the πd channel and a ratio of ~ 0.04 (~ 0.17) for the $^3F_3$ state. This fact is consistent with the conclusion for the NN system as shown in Table 1.

We note here that based on the $p^{\uparrow}p^{\uparrow} \rightarrow \pi^+d$ data[31,32,34] the existence of dibaryons was doubted. However, this doubt does not seem valid because the above-mentioned phase-shift analysis gives a reasonable χ^2/NDF value. We expect updated $pp \rightarrow \pi d$ phase-shift results soon.

The existence of a resonant state in the pp system at the approximate energy of 2.7 GeV was suggested by the result of measurements in $p^{\uparrow}p^{\uparrow} \rightarrow d\pi^+$ at T_p = 1.2 to 2.3 GeV.[35] The angular distributions of the analyzing power as shown in Fig. 8 indicate a strong energy dependence. Structures found in similar energies are discussed earlier.

2.5 Inclusive Reactions

Apart from the broad structure observed in the B = 2 system (see earlier sections), a considerable amount of experimental work has been devoted to the study of narrow resonances.[36] Theoretically, the interest in narrow resonances $\Gamma_{1/2} \leq 100$ MeV was stimulated by the possibility that the quark color degree of freedom might manifest itself in the form of exotic states with narrow width in the B = 2 system. In the T = 1 channel the first observations of such states in the $p^3He \rightarrow dX$ in Saturne experiments[37] above the NN π threshold were confirmed by analyzing powers deduced from an experiment, $p^{\uparrow}{}^3He \rightarrow dX$, at an incident proton energy of 80 MeV performed recently at LAMPF.[38] The analyzing powers, A_y, are shown in Fig. 9. A dummy target consisting of an empty cell replacing the liquid ^3He cell was used to account for the deuterons produced in the target cell. Table 2 summarizes the results of Saturne II and LAMPF experiments, together with predictions of theoretical models.

An experimental search for B = 2, T = 2 bound states in the vicinity of the πNN threshold was conducted in the $pp^{\uparrow} \rightarrow \pi^-X$ reaction.[44]

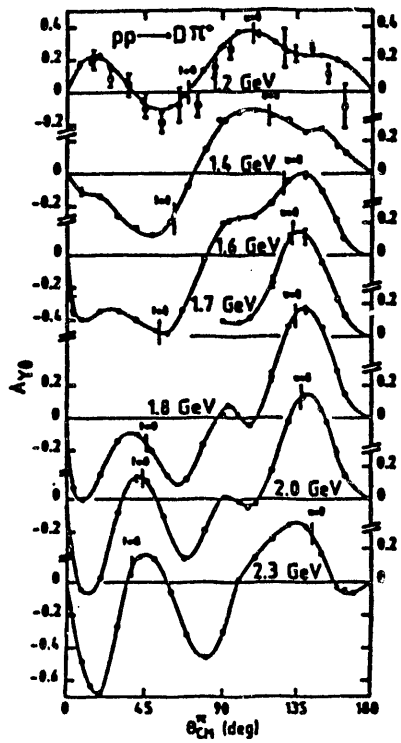

Figure 8. Angular distribution of the analyzing power.

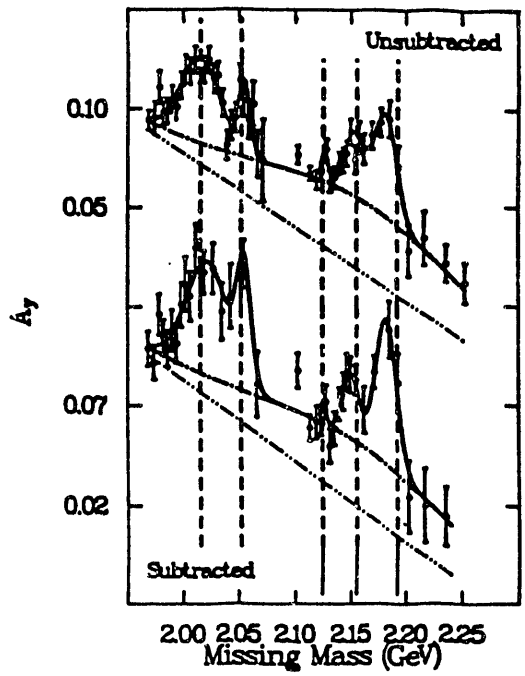

Figure 9. Analyzing powers in p↑3He → dX before and after dummy target subtraction.

Table 2. Narrow Structures in the B = 2 System.

LAMPF		Saturne II		Rotational Formula[39]	Bag Model[40]
Peak Position (MeV)	FWHM (MeV)	Peak Position (MeV)	FWHM (MeV)	Resonance Mass	Resonance Mass × 0.9
2015 ± 5	34 ± 14			2015	2015, 2017
2054 ± 4	11 ± 6			2052	2098, 2100
2125 ± 3	6 ± 7	2124 ± 3	25 ± 2	2124	2121, 2129
2152 ± 4	20 ± 10			2155	2164
2181 ± 5	20 ± 8	2192 ± 3	25 ± 6	2192	2175, 2180, 2185

2.6 A Narrow-Width Dibaryon as ηNN Quasi-Bound State

The possibility of the existence of πNN bound states has been suggested. Since strong attraction due to the πN interaction in the P_{33} state and the NN interaction in the $^3S_1$ state exists in the system, a bound state has been expected there. However, the large centrifugal repulsion in the P_{33} resonance makes it difficult for the system to be bound. Thus, rather than a bound state, resonance states exist in the πNN system. $J^P = 2^+$ and $J^P = 3^-$ resonances are theoretically predicted, and are in agreement with the experimental data.

In the ηNN system, the important interactions are the ηN - πN interaction in the S_{11} state and the NN interaction in the $^3S_1$ state. Both interactions give no centrifugal repulsion providing a greater possibility for a bound ηNN state.

The existence of an I = 0, $J^P = 1^-$ quasi-bound state in the ηNN-πNN coupled system is theoretically predicted with a mass of about 2430 MeV and a width of 10-20 MeV.[42]

It was observed that the np ($^1P_1$) → np ($^1P_1$) amplitude shows anticlockwise looping as shown in Fig. 10.

3. Proton-Proton Elastic Scattering at High $p_\perp$

Earlier studies on proton-proton (pp) elastic scattering are summarized, Refs. 1 and 2. With polarized-proton beams at BNL, the analyzing power, A_N, and spin-spin correlation parameter, A_{NN}, were measured[43] up to incident proton-laboratory momentum of 24 GeV/c and $p_\perp^2$ up to 7.1 $(GeV/c)^2$. As shown in Fig. 11, values of A_N increase as $p_\perp^2$. A similar trend is observed in the hadron production which will be described later.

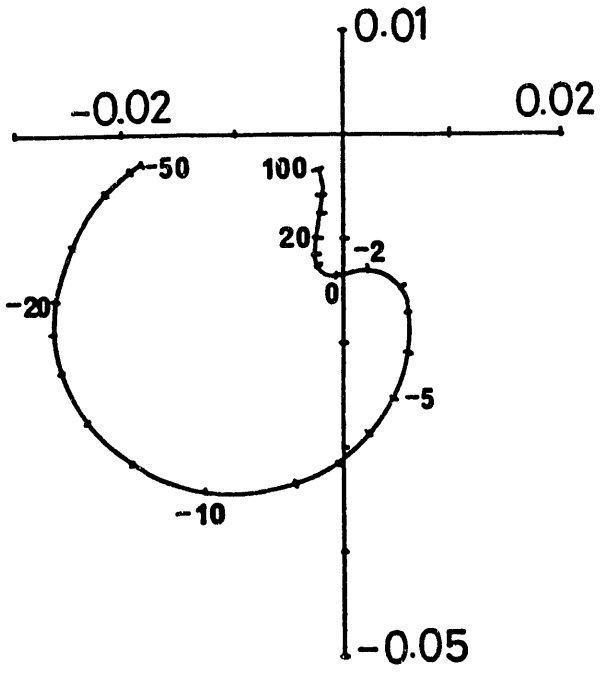

Figure 10. np ($^1P_1$) → np ($^1P_1$) amplitude.

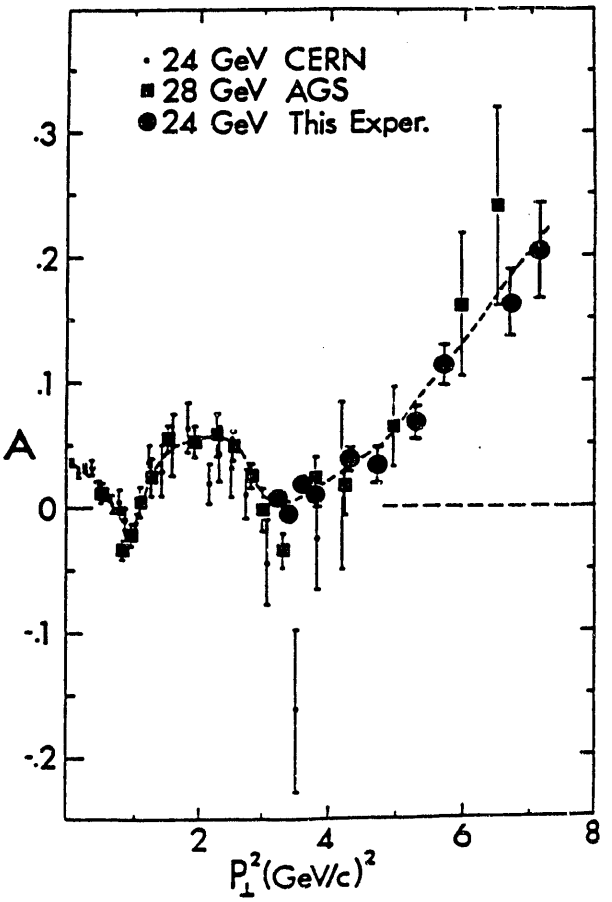

Figure 11. A_N in pp elastic scattering.

4. Polarization of Hyperons

The high-energy hyperon polarization data come from inclusive reactions. The Λ polarization in the proton fragmentation region has been thoroughly investigated. It appears to be almost independent of energy, from CERN PS (or AGS) to ISR energies. At low $p_\perp$ the polarization has a weak x_F dependence, but for $p_\perp > 1$ GeV/c the polarization increases linearly with x_F.

The polarizations of other hyperons have been measured as well. The polarization of the cascade particles is about the same as that of the Λ, and the Σ polarization has opposite signs to that of the Λ but about the same magnitude.

All of these experimental findings have been parametrized by combining the fragmentation picture with SU(6) symmetry, which amounts to the assumption that valence quarks carry all the spin of the proton.[44,45] The data were also qualitatively explained by a model using mass-corrected perturbative QCD.[46] The problem of explaining, within the framework of PQCD, the large observed single transverse-spin asymmetries in hyperon production was reviewed.[47] The absence of small parameters in the first-order asymmetry in QCD was stressed.[48]

The cross sections for $p\,B_e \rightarrow \Lambda X$ and $\Sigma^\circ X$ have been measured[49] at a beam momentum of 28.5 GeV/c at an average laboratory production angle of 4°. The ratio $\sigma(\Sigma^\circ)/\sigma(\Lambda)$ was $0.278 \pm 0.011 \pm 0.05$, where the uncertainties are statistical and systematic in that order. The ratio does not depend strongly on the momentum of the produced particle measured earlier between 10 and 24 GeV/c. It does not agree with any of the theoretical predictions for this ratio. For example, a calculation7 based on SU(6) formalism and polarization measurements predicts 0.11. Interestingly, it may be argued that Σ and Λ productions should be equal. Since there are three Σ's, $\Sigma^\circ/\Lambda^\circ$ should be roughly one-third. Thus, SU(6) appears to be severely broken, although the ratios of cross sections for exclusively produced $Y\bar{Y}$ pairs in $p\bar{p}$ collisions are within 10-20% in agreement with SU(6).

The large ratio $\sigma(\Sigma^\circ)/\sigma(\Lambda)$ implies that a substantial fraction of the Λ's observed experimentally are decay products of Σ°. The polarization of the Σ° in $p\,B_e \rightarrow \Sigma^{\circ\uparrow} + X$ at 28.5 GeV/c was measured[50] to be 0.28 ± 0.13 at an average $p_\perp = 1.01$ GeV/c and $x_F = 0.60$. This value is in good agreement with 0.23 ± 0.13 measured[51] at 18.5 GeV/c. The polarization of direct Λ's may be diluted by decay Λ's. The direct Λ polarization is substantially greater than the already large values that have been measured.

4.1 Polarization and Magnetic Moment of $\bar{\Xi}^+$ Antihyperons

The polarization of $\bar{\Xi}^+$ hyperons produced by 800 GeV/c protons in the inclusive reactions $p + Be \rightarrow \bar{\Xi}^+ + X$ is approximately equal to that of Ξ^- as shown in Fig. 12.[52] Models

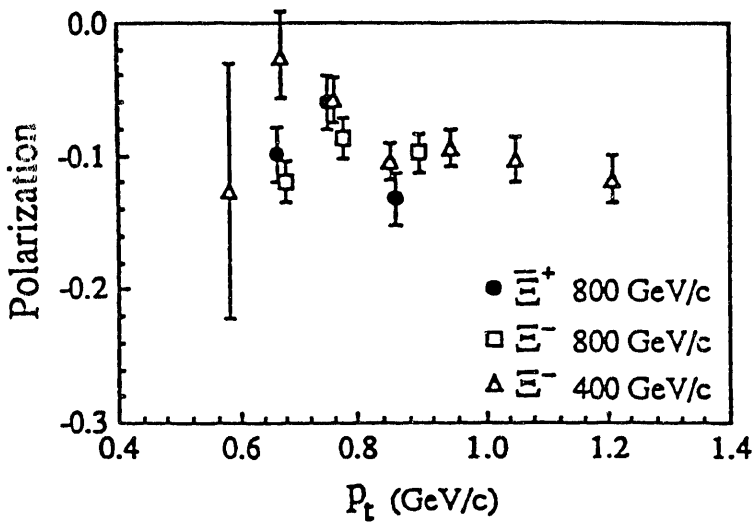

Figure 12. Comparison of the $\bar{\Xi}^+$ and Ξ^- polarization with that of the Ξ^- data taken at 400 GeV/c and a production angle of 5 mrad.

predict zero polarization for all antihyperons, as polarization of $\bar{\Lambda}$'s produced protons found to be consistent with zero. Non-zero polarization of $\bar{\Xi}^+$ calls into question those models. The presence of a significant polarization for the $\bar{\Xi}^+$ makes possible the first measurement of the magnetic moment of an antihyperon. It was determined to be $\mu_{\bar{\Xi}^+} = 0.657 \pm 0.028 \pm 0.020$ nucleon magnetrons.[52]

4.2 Polarization and Magnetic Moment of Ω^-

By a polarized neutral beam from $p + Cu \rightarrow (\Lambda, \Xi^0)^\uparrow + X$, Ω^- hyperons were produced in a spin-transfer reaction, $(\Lambda, \Xi^0)^\uparrow + Cu \rightarrow \Omega^- + X$.[53] The Ω^- polarizations are found to be -0.054 ± 0.019 and -0.149 ± 0.055 at mean Ω^- momenta of 322 and 398 GeV/c, respectively. Based on these polarizations, the Ω^- magnetic moment is determined to be $(-1.94 \pm 0.17 \pm 0.14)\ \mu_N$, in good agreement with the naive-quark-model prediction of $-1.84\ \mu_N$.[54]

4.3 Polarization of Ξ^- Hyperons

The polarization P_{Ξ^-} of Ξ^- hyperons produced by 800-GeV protons was measured for x_F from 0.3 to 0.7 and $p_\perp$ from 0.5 to 1.5 GeV/c.[55] The kinematic behavior of P_{Ξ^-} is shown in Fig. 13. The Ξ^- polarization does not demonstrate the strong x_F dependence shown by P_Λ. Also, an energy dependence of P_{Ξ^-} was observed; $|P_{\Xi^-}|$ at 800 GeV/c is larger than that of 400 GeV/c as shown in Fig. 13.

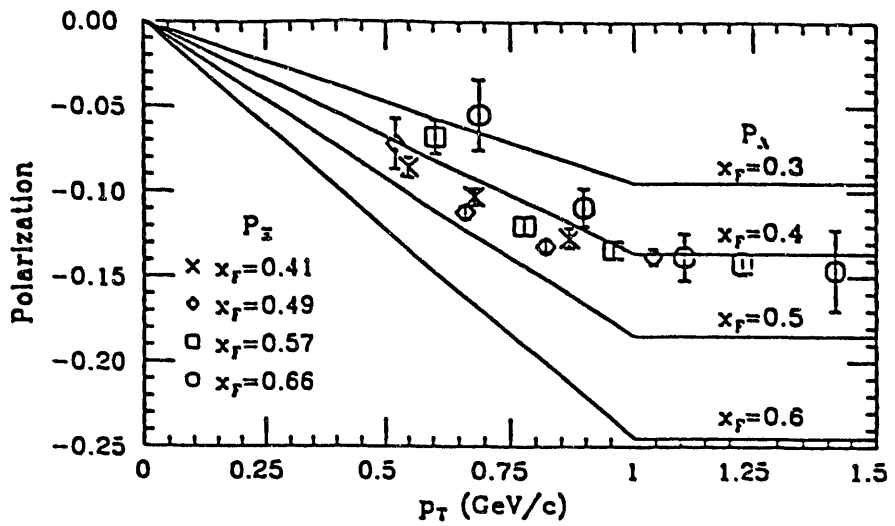

Figure 13. P_{Ξ^-} as a function of p_T for contours of constant average x_F. The lines are a schematic representation of the behavior of the Λ polarization from $x_F = 0.3$ to $x_F = 0.6$, the same region as the P_{Ξ^-} results.

5. Polarized Beams at Fermilab

5.1 Introduction

Ever since polarized beams and/or polarized targets became available for the use of high-energy experiments, various measurements on the polarization phenomena have been extensively carried out. Asymmetry measurements are sensitive to interference terms between dominant and nondominant amplitudes, and thus provide useful information which cannot be obtained from

differential cross section measurements alone, on the study of production and reaction mechanisms.

The physics objectives for the Fermilab polarized beam facility up to 200 GeV/c were in part based upon the facts that there were already several experimental indications that spin effects are significant at high energy. They were

i) Measurements of π° production at high $p_\perp$ ($p_\perp > 2.0$ GeV/c) in proton-proton at CERN and in π^- proton collisions at Serpukhov revealed sizable asymmetries at 24 GeV/c and 40 GeV/c, respectively.

ii) Hyperons produced at large x_F inclusively off nuclei and hydrogen at CERN, Fermilab, and ISR, were observed to have high polarizations.

iii) Inelastic scattering of longitudinally polarized electrons on longitudinally polarized protons at SLAC yielded a large asymmetry, implying that proton helicity orientation is communicated to the constituent quarks. Thus, spin dependence in quark-quark collisions can be inferred from measurements of spin dependence in proton-proton collisions in appropriate kinematic regions.

The observation of these large effects suggested that the underlying processes involved might be simple at the level of constituents. A number of theoretical models were introduced to explain these polarization phenomena and predictions for future measurements were made.

5.2 Polarized Beam (protons and antiprotons) Facility

During the last decade, construction of a high-energy (above 100 GeV/c) polarized beam was attempted. In order to avoid possible complications involving depolarization at high energies, polarized protons can be produced from decaying hyperons, lambdas, or sigmas. The Fermilab polarized-beam facility was constructed and was operational in 1987.

An extracted beam from the Tevatron is delivered through the MP primary-beam line to the Meson Detector Building where a 0.73-interaction-length Be target is utilized to produce Λ and $\bar{\Lambda}$ at $\theta_{c.m.} \approx 0^\circ$. Protons and antiprotons from the Λ and $\bar{\Lambda}$ decays respectively are brought to a final target position in the MP hall through the MP secondary beam (200 GeV/c) line.

Polarized protons from the virtual sources are focused in the tagging section, where both the momentum and polarization are selected.[56] The typical beam flux ($\Delta p/p = \pm 5\%$) for 3×10^{12} incident protons per 20-sec spill at 200 GeV/c were: (P_{av} is average polarization)

	Tagged Beam ($P_{av} = 45\%$)	Total Particles	Background π's
Protons	1.0×10^7	2.0×10^7	2.0×10^6
Antiprotons	5.0×10^5	1.0×10^6	5.0×10^6

5.2.1 Primakoff-Effect Measurement

The asymmetry of the nuclear coherent Coulomb π° production process ("Primakoff Process"), was measured[57] for the first time with the use of the 200-GeV/c polarized-proton beam. The apparatus consisted of a lead-glass calorimeter for π° detection and a magnetic spectrometer for the scattered protons. A large asymmetry in the region of $|t'| < 0.001$ $(GeV/c)^2$ and $1.36 < M(\pi^\circ p) < 1.52$ GeV/c^2 was observed for the reaction $p + Pb \rightarrow p + \pi^\circ + Pb$, where the Coulomb process is predominant.

The measured asymmetry for the Coulomb process is consistent with the analyzing power (about -70%) of the π° production process deduced from existing low-energy $\gamma + p^\uparrow \rightarrow \pi^\circ + p$ data. The results demonstrate that the Primakoff process is useful as a polarimeter for high-energy polarized beams.

5.2.2 Coulomb-Nuclear Interference (CNI) Measurement

Several authors since Schwinger[58] have indicated nonzero polarization in the Coulomb-nuclear interference region in nucleon-nucleon scattering. This polarimeter is to measure the interference term of the nonflip amplitude and the electromagnetic spin-flip amplitude. The proton polarization arising from the interference is $P \approx 5\%$ at $|t| = 2 \cdot 10^{-3}$ $(GeV/c)^2$ and is energy independent.[59]

The analyzing power, A_N, of proton-proton, proton-hydrocarbon, and antiproton-hydrocarbon scattering in the Coulomb-nuclear region was earlier measured using the 200-GeV/c polarized beams.[60] The results at $|t| \sim 0.003$ $(GeV/c)^2$ show the value $A_N = (2.4 \pm 0.9)\%$ with the polarized-proton beam, and $A_N = (-4.6 \pm 1.9)\%$ with the polarized-antiproton beam both on a hydrocarbon target, and also $A_N = (4.5 \pm 2.8)\%$ of proton-proton scattering. These results are consistent with predictions[61-63] based on Coulomb-nuclear interference.

Recently a new CNI target consisting of trans-stilbene crystals (diphenyl-ethylene, $C_{14}H_{12}$) was used.[64] Large background was reduced at small $|t|$ region by using this material that possesses pulse-shaped discrimination characteristics. Preliminary results on the pp analyzing power are shown in Fig. 14 together with the calculated values.

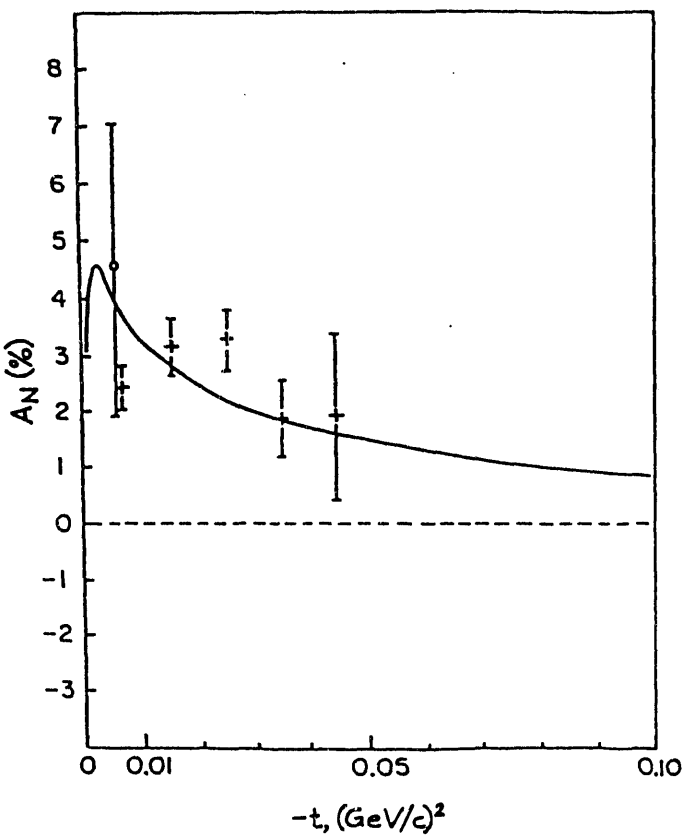

Figure 14. pp analyzing power in the Coulomb-nuclear region.

5.3 Hadron Production with 200-GeV/c Polarized Proton and Antiproton Beams

5.3.1 Single-Spin Asymmetry in $p^{\uparrow}p \rightarrow (\pi^{\circ}, \eta)$ and $\bar{p}^{\uparrow}p \rightarrow \pi^{\circ}X$ at high $p_{\perp}$

Asymmetry measurements, $A_N = (1/P_B)(N^{\uparrow} - N^{\downarrow})/(N^{\uparrow} + N^{\downarrow})$, were carried out at 200 GeV/c in π° and η production. Photons from the decay of π°s produced in the target are detected in the "Central Electromagnetic Calorimeters" CEMC-1 and CEMC-2, shown in Fig. 15, located symmetrically to the left and to the right of the beam axis at 10 m from the target. Each calorimeter is comprised of 504 lead-glass counters in an array of 21 columns by 24 rows. The dimensions of each lead-glass block are 3.81 cm × 3.81 cm × 18 radiation lengths. Each array covers polar angles of $(5.5 \pm 2.2)^{\circ}$ in the laboratory frame, where 5.5° corresponds to 90° in the c.m., and azimuthal angles of ± 25° with respect to the horizontal plane containing the beam axis.

Data of the $p^{\uparrow}p$ reaction[65] show that the asymmetry values (A_N) at $x_F \approx 0$ are approximately zero (or small negative) up to $p_{\perp} = 3.5$ GeV/c and then begin to rise to ~ + 40% in the region of $p_{\perp} = 4$ to 5 GeV/c as shown in Fig. 16.

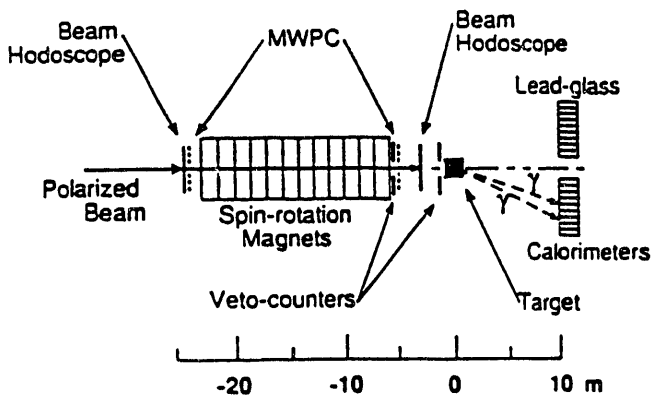

Figure 15. Layout of the experimental apparatus.

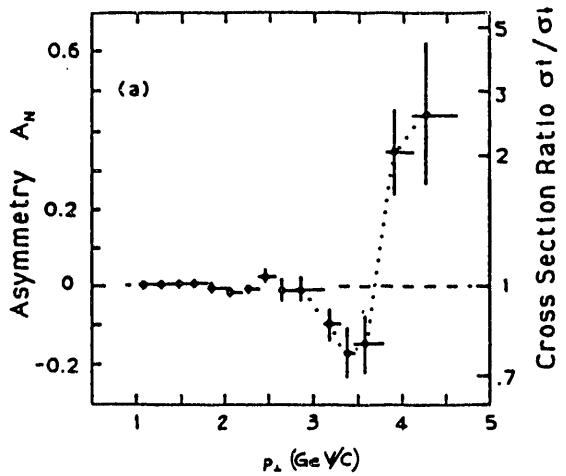

Figure 16. $p_{\perp}$ dependence of A_N at $x_F = 0$.

At lower energies as seen in the BNL[66] ($p^{\uparrow}p \rightarrow \pi^{+}X$), CERN[67] ($pp^{\uparrow} \rightarrow \pi^{\circ}X$), Serpukhov[68] ($\pi^{-}p^{\uparrow} \rightarrow \pi^{\circ}X$) data, this rapid rise from zero to large positive values, was also observed although none of the data exceeded $p_{\perp} = 3$ GeV/c. A positive sign of A_N mentioned above corresponds to a larger production cross section to beam-left (beam-right) when the beam (target) proton is vertically-upward. Note that for the usual sign convention, $A_N (p^{\uparrow}h \rightarrow hX) = -A_N (hp^{\uparrow} \rightarrow hX)$ at $x \approx 0$ where h represents hadron. A new finding is that all the A_N data of π° or π^{+} production at $x_F \approx 0$ show the large positive asymmetries begin at $x_{\perp} = 0.4$ in the region $\sqrt{s} = 5$ to 20 GeV as shown in Fig. 17. This is strong indication that we are indeed observing asymmetries caused by hard scattering.

Single-spin asymmetry in $\bar{p}^{\uparrow}p \rightarrow \pi^{\circ}X$ shows a similar $p_{\perp}$ dependence as the $p^{\uparrow}p$ case. However, data are limited only up to $p_{\perp} = 3.5$ GeV/c as shown in Fig. 18a. We have also observed a similar $p_{\perp}$ dependence in $p^{\uparrow}p \rightarrow \eta X$ as shown in Fig. 18b.

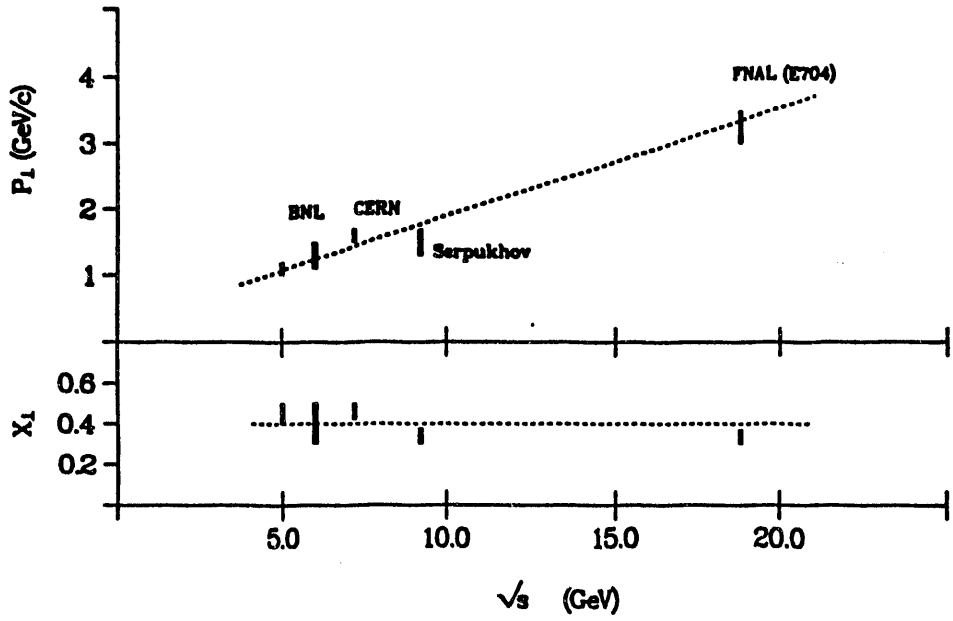

Figure 17. Onset of structure in A_N vs. $\sqrt{s}$.

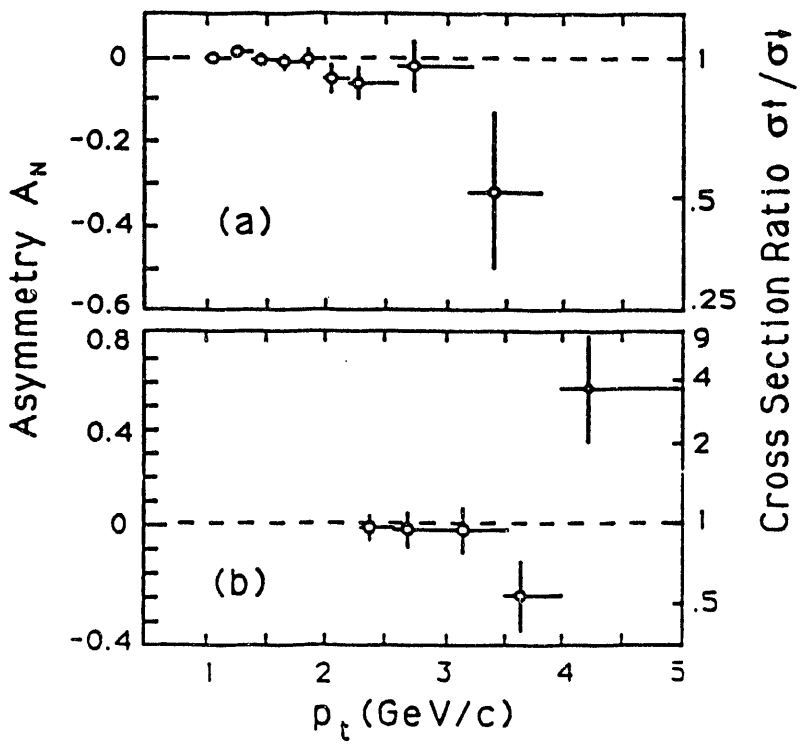

Figure 18. (a) $p_\perp$ dependence of A_N in $\bar{p}p \rightarrow \pi^0 X$.
(b) $p_\perp$ dependence of A_N in $pp \rightarrow \eta X$.

5.3.2 *x_F Dependence of Single-Spin Asymmetry in $p^{\uparrow}p \rightarrow \pi^{\circ}X$ and $\bar{p}^{\uparrow}p \rightarrow \pi^{\circ}X$*

Asymmetry measurements (A_N) in $p^{\uparrow}p \rightarrow \pi^{\circ}X$ and $\bar{p}^{\uparrow}p \rightarrow \pi^{\circ}X$ on the x_F dependence at 200 GeV/c covering $p_\perp$ up to 2 GeV/c were carried out.[69] A_N values in the $p^{\uparrow}p$ reaction are consistent with zero up to $x_F = 0.3$ to 0.4, and then linearly increase to + 20% near $x_F = 1.0$ as shown in Fig. 19. Also they are consistent with earlier data[70] taken at $\langle x_F \rangle = 0.52$.

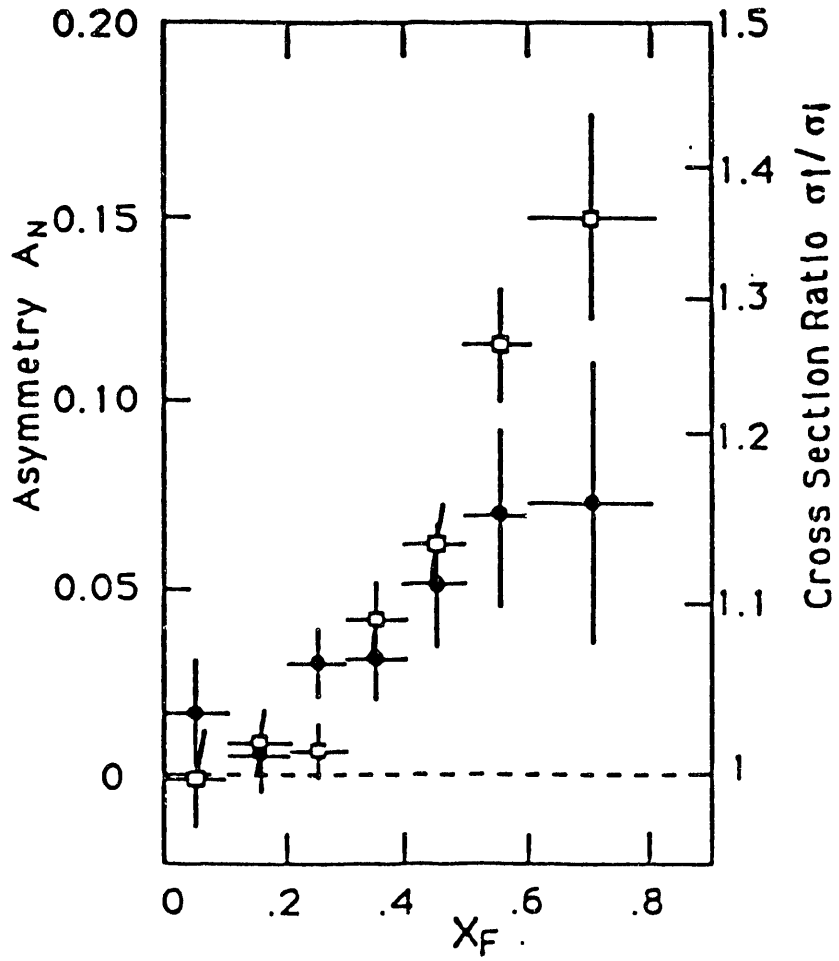

Figure 19. x_F dependence of A_N at $p_\perp$ = 0.5 to 2.0 GeV/c in the reaction $p^{\uparrow}p \rightarrow \pi^{\circ}X$ (open squares) and $\bar{p}p \rightarrow$ (closed circles).

Single spin asymmetry in $\bar{p}^{\uparrow}p$ reaction shows a similar x_F dependence as $p^{\uparrow}p$ case. By knowing the quark content of $\pi^{\circ} = (u\bar{u} - d\bar{d})/\sqrt{2}$, both the polarized u and $\bar{u}$ quark in the polarized proton and antiproton beam respectively seen to be the career of the spin information. We can also interpret these results using a dynamical mechanism[71] describing the spin effect in the inclusive hadron production in the fragmentation region. In this mechanism, asymmetries in $pp \rightarrow \pi^{\circ}X$ and $\bar{p}p \rightarrow \pi^{\circ}X$ are related to the πp backward scattering as i) $\pi^{\circ}p \rightarrow p\pi^{\circ}$ and ii) $\pi^{\circ}\bar{p} \rightarrow \bar{p}\pi^{\circ}$, respectively. By applying the CPT conservation, the antiprocess of the i) is the process ii). Thus, similar x_F dependence in asymmetries by protons and antiprotons can be explained.

It is interesting to notice that our data resembled x_F dependence in $pp \rightarrow \Lambda^{\uparrow}X$ where polarized s quarks were considered[72] to be responsible for high polarization.

We also present the ratio of the spin-averaged cross sections for π^o production by antiprotons and by protons as shown in Fig. 20.

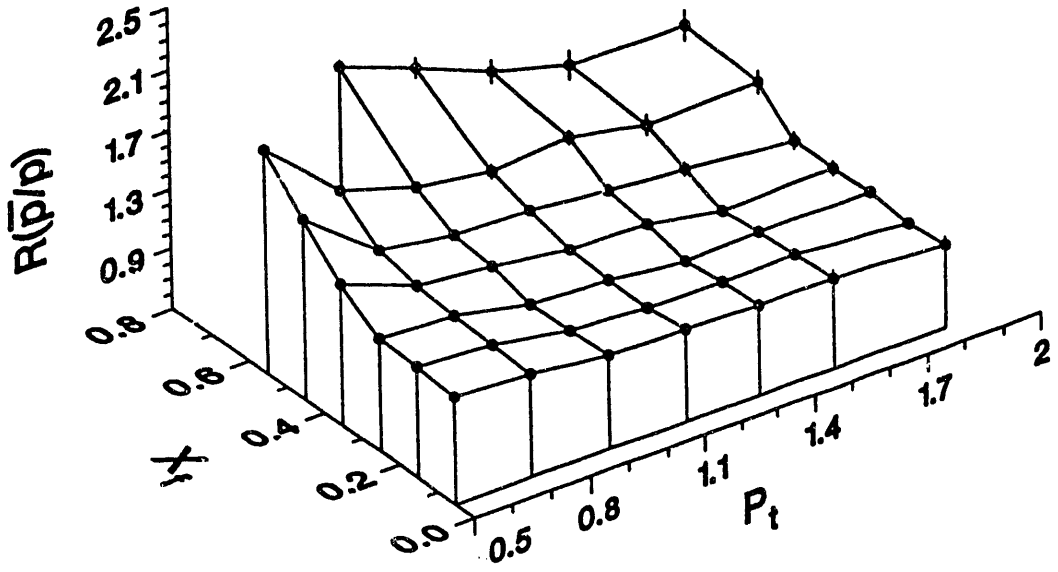

Figure 20. The ratio $R(\bar{p} / p)$ of the cross section for π^o production by antiprotons and by protons.

5.3.3 x_F Dependence of Single-Spin Asymmetry in $p^{\uparrow}p \rightarrow \pi^{\pm} X$ and $\bar{p}^{\uparrow}p \rightarrow \pi^{\pm}X$

Single-spin asymmetries were measured in $\pi^{\pm}$ production at 200 GeV/c.[73] Pion production from the target was measured via a large forward spectrometer which is shown in Fig. 21. The asymmetry values (A_N) in the $p^{\uparrow}p$ reaction are shown in Fig. 22 as a function of x_F for the π^+ and π^- data over a $p_\perp$ range of 0.2 - 2.0 GeV/c. The data exhibit a striking form in which the magnitude of A_N increases for both π^+ and π^- particles with x_F, but the sign of A_N is negative for the π^- data. Further study of these data shows a threshold effect in which A_N increases dramatically above $p_\perp$ = 0.7 GeV/c.

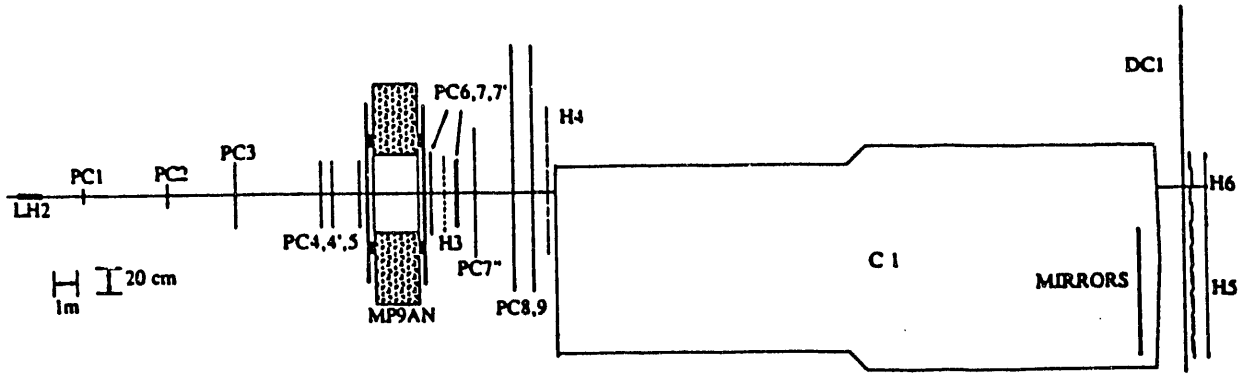

Figure 21. Top view of the E-704 forward spectrometer layout.

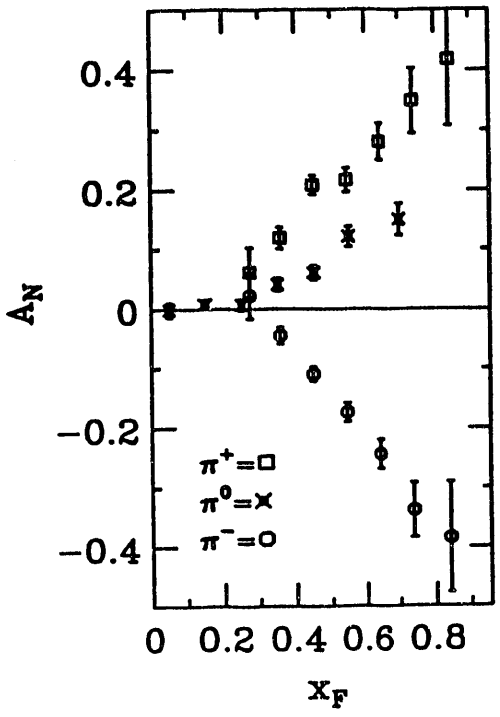

Figure 22 A_N for π^+ (squares) and π^- (circles) production in the $p^\uparrow p$ reaction versus x_F integrated over $p_\perp$. For comparison, π^0 data (crosses) are also plotted.

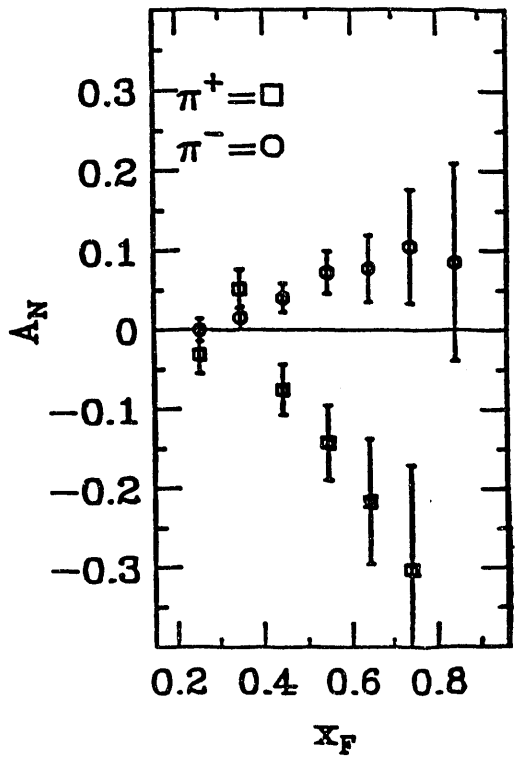

Figure 23. A_N for π^+ (squares) and π^- (circles) in the $\bar{p}^\uparrow p$ reaction.

From this mirror-symmetry effect in π^+ and π^-, one may speculate $A_N = 0$ for π° production. By applying isospin relations for single-particle distributions,[74] $\sigma^+ A_N^+ + \sigma^- A_N^- = 2\sigma^\circ A_N^\circ$, where σ^+ and A_N^+ are for the cross section and analyzing power in $p^\uparrow p \to \pi^+ X$ respectively, σ^- and A_N^- in $p^\uparrow p \to \pi^- X$, and σ° and A_N° in $p^\uparrow p \to \pi^\circ X$, we can conclude the following: Experimental data show $\sigma^+ > \sigma^-$ and $A_N^+ \approx -A_N^-$, therefore we expect $A_N^\circ > 0$ as shown in Fig. 19.

The A_N values in the $\bar{p}^\uparrow p$ reaction[75] are shown in Fig. 23 for the π^+ and π^- data. We observe a similar behavior on A_N magnitude with respect to x_F but the sign of A_N is positive for the π^- data and negative for the π^+ data. The results can be explained by using the model[71] which relate $pp \to \pi^\pm X$ scattering to the πp backward scattering. The antiprocesses of $\pi^+ p \to p\pi^+$ and $\pi^- p \to p\pi^-$ are $\pi^- \bar{p} \to \bar{p}\pi^-$ and $\pi^+ \bar{p} \to \bar{p}\pi^+$ respectively. Thus we have opposite signs for $p^\uparrow$ and $\bar{p}^\uparrow$ beams.

5.3.4 Summary of $x_\perp$ and x_F Dependence

There are two distinct common phenomena observed in the $x_\perp$ and x_F dependence of the one-spin asymmetries. The asymmetry values are zero or small for both $x_\perp$ and $x_F < 0.3$ to 0.4. Then there is a rise from zero to large positive values for $x_\perp$ and $x_F > 0.3$ to 0.4. It will be interesting to find out if these two phenomena are related.

A recent review[76] discusses the various theoretical approaches used to explain the possible origin of single-spin asymmetries in pion production. According to Ref. 77, the possible

origin is an asymmetry in the transverse-momentum distributions, due to orbital angular momentum of the constituents in a polarized proton. An alternate suggestion[78] invokes transverse forces that are generated when rotating color charges in the spinning proton interact with the gluon field of the target. The most recent attempt[79] to describe single-spin transverse spin asymmetries at $p_T > 3$ GeV/c is made by introducing the leading contribution from a spin dependent quark-gluon correlation function ("twist-3" parton distribution) in perturbative QCD.

5.3.5 Single Spin Asymmetry in Direct Photon Production

In addition to the calorimeter used for the π° production discussed above, a lead-scintillator sandwich counter (called guard counter) that surrounds the calorimeter was placed to increase the acceptance for the direct γ.

As will be discussed in Section 7.3, A_N measurements in direct photon production provided information on the twist-3 parton distribution involving the correlation between quark and gluon field strength (presented by N. Saito at the Nagoya Symposium).

5.3.6 Double-Spin Asymmetry in π° Production

We report on a first measurement of the two-spin parameter A_{LL} for inclusive π° production by 200-GeV longitudinally-polarized protons and antiprotons on a longitudinally-polarized proton target. The hadron asymmetry A_{LL} is defined as the relative difference between the cross sections for beam and target hadrons of equal or opposite helicities,

$$A_{LL} = (\sigma^{\rightleftarrows} - \sigma^{\rightrightarrows}) / (\sigma^{\rightleftarrows} + \sigma^{\rightrightarrows})$$

$$= P_B^{-1} \bullet < P_T >^{-1} \bullet \left(N^{\rightleftarrows} - N^{\rightrightarrows}\right) / \left(N^{\rightleftarrows} + N^{\rightrightarrows}\right),$$

where $\sigma(s, x_F, p_t)$ are the invariant cross sections for inclusive π° production in antiparallel ($\rightleftarrows$) and parallel ($\rightrightarrows$) spin states of the beam and target particles. Since the incident hadrons have opposite momenta in the c.m. of the interaction, the helicities are equal when the spin directions are not parallel. The quantities $N(s, x_F, p_t)$ are the corresponding normalized event rates measured in the experiment, P_B is the beam polarization, and $<P_T>$ is the target polarization averaged over polarized and unpolarized nucleons.

The 3-cm diameter polarized proton target[80] of length 20 cm consists of 2-mm diameter beads of frozen Pentanol ($C_5H_{12}O$) doped with Chromium-V. Pentanol contains one polarizable, free proton for about six unpolarizable, bound protons and neutrons. The effective polarization-dilution factor, including the target windows, is $D = P_T/<P_T> = (8 \pm 1)$. The free protons are polarized to typically either $P_T = 0.75$ or $P_T = -0.80$ in 3 to 4 hours at a temperature of 0.4K, using microwaves of appropriate frequencies near 70 GHz.

The results[81] for A_{LL} measured for incident protons and antiprotons as a function of $p_\perp$, are shown in Fig. 24. Each value for A_{LL} in the $p_\perp$ interval covered by these measurements is consistent with zero, within the statistical errors.

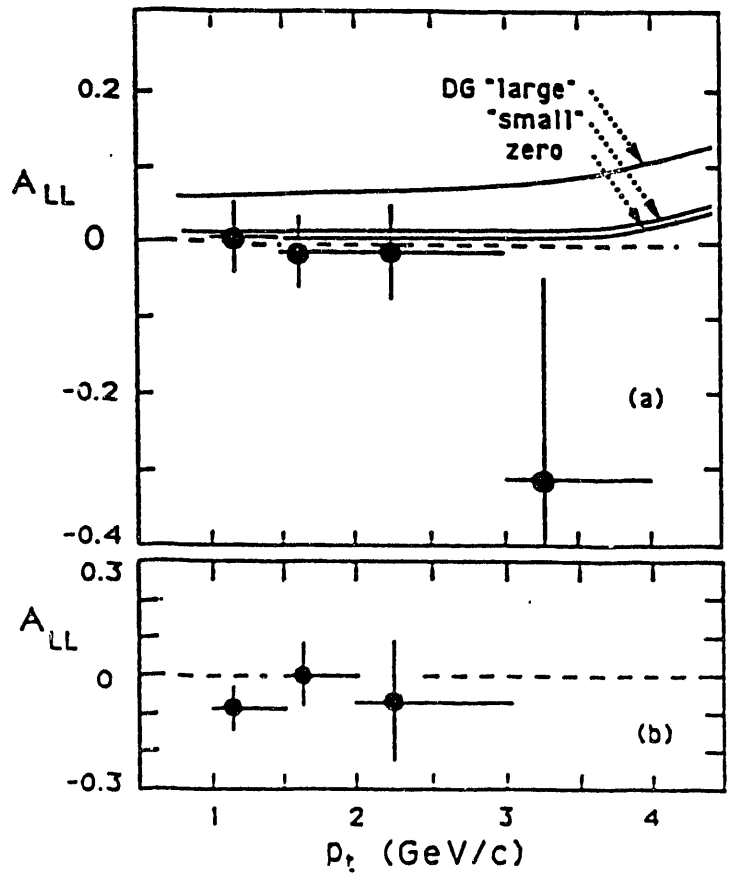

Figure 24. The two-spin parameter A_{LL} in the reaction (a) $pp \rightarrow \pi^o X$ and (b) $pp \rightarrow p^o X$ at 200 GeV/c, for $-0.1 < x_F < 0.1$. The curves are predictions for different values of the spin-weighted gluon distribution function (see Ref. 82).

5.4 One-Spin and Two-Spin Measurements in Λ Production

Many experiments have measured polarization values for various hyperons (Λ, Σ^+, Σ^-, Σ^o, Ξ^o, Ξ^-, and Ω^-). The data exhibit a certain simple pattern as: i) all hyperons produced by proton fragmentation are polarized perpendicular to the production plane but anti-hyperons are not, ii) the magnitude of the polarization increases linearly with p_T below p_T of 0.8 GeV/c, is independent of p_T above 1 GeV/c, and increases linearly with x_F, and iii) the polarization is independent of energy.

To explain these spin effects many have proposed a wide range of mechanisms but none of them completely explains all the data. At 200 GeV/c, three parameters were measured for further understanding of Λ asymmetry effects; they are the polarization P, the analyzing power A, and the depolarization D.

$$P = \left(\sigma_f^{\uparrow} - \sigma_f^{\downarrow}\right) / \left(\sigma_f^{\uparrow} + \sigma_f^{\downarrow}\right),$$

$$A = (1/P_B)\left(\sigma_i^{\uparrow} - \sigma_i^{\downarrow}\right) / \left(\sigma_i^{\uparrow} + \sigma_i^{\downarrow}\right),$$

and $$D = (1/P_B)[\sigma(i//f) - \sigma(i\not\!/\, f)]/[\sigma(i//f) + \sigma(i\not\!/\, f)$$

5.5 Difference in Total Cross Sections, $\Delta\sigma_L$

The difference between total cross sections with spins antiparallel and with spins parallel longitudinally was measured at 200 GeV/c.

$$\Delta\sigma_L = \left[\sigma^{Tot}\left(\rightleftarrows\right) - \sigma^{Tot}\left(\rightrightarrows\right)\right].$$

The values of $\Delta\sigma_L$ was -16 mb at ~ 1.5 GeV/c incident proton momentum where $\sigma^{Tot} \sim 40$ mb. For pp the part that survives at high energy is expected to come from A_1 exchange and this scales roughly as $1/P_{lab}$. The prediction at 200 GeV/c is -50 μb. For $\bar{p}p$ there may be a large contribution that amount to ~ 2 mb due to $q\bar{q}$ annihilation.

Total cross-section measurements at lower energies are usually made in a geometry close to a pencil beam, a point-like target, and detectors defining concentric rings for the extrapolation of the transmission rates to zero solid angle.

For the measurement at 200 GeV/c, the beam divergence was relatively large and the position and direction of the particles incident on the target is defined by two hodoscopes. Two different transmission hodoscopes, DSL1 and DSL2, were placed at 16m and 47m respectively from the target. Results of DSL1 and DSL2 were analyzed by a Saclay group and DSL1 is being analyzed by an Argonne group. Preliminary results by the Saclay group are shown in Fig. 25, where systematic and statistical errors are combined.

6. Recent Results from IHEP, Serpukhov (Presented by S. Nurushev at the Nagoya Symposium)

6.1 Single-Spin Asymmetry in the Reaction $\pi^- d^{\uparrow} \rightarrow \pi^0 X$ at 40 GeV/c

The single-spin asymmetry A_N in the inclusive reaction $\pi^- d^{\uparrow} \rightarrow \pi^0 X$ in the beam fragmentation region at 40 GeV/c was measured. A frozen-spin ($C_3D_8O_2$) polarized target was used. The p_T dependence of the A_N was observed as similar to the one in case of hyperon polarization over the interval $0.7 < x_F < 0.9$.

6.2 Preliminary Results on the Asymmetry in $pp^{\uparrow} \rightarrow \pi^0 X$ at 70 GeV/c at $x_F = 0$

A 70-GeV/c proton beam was produced by means of a bent crystal which was installed inside the vacuum tube of the Serpukhov accelerator.

Single-spin asymmetry A_N was measured up to 4 GeV/c. The data are compared with earlier data with different energies at CERN, BNL, Serpukhov, and Fermilab.

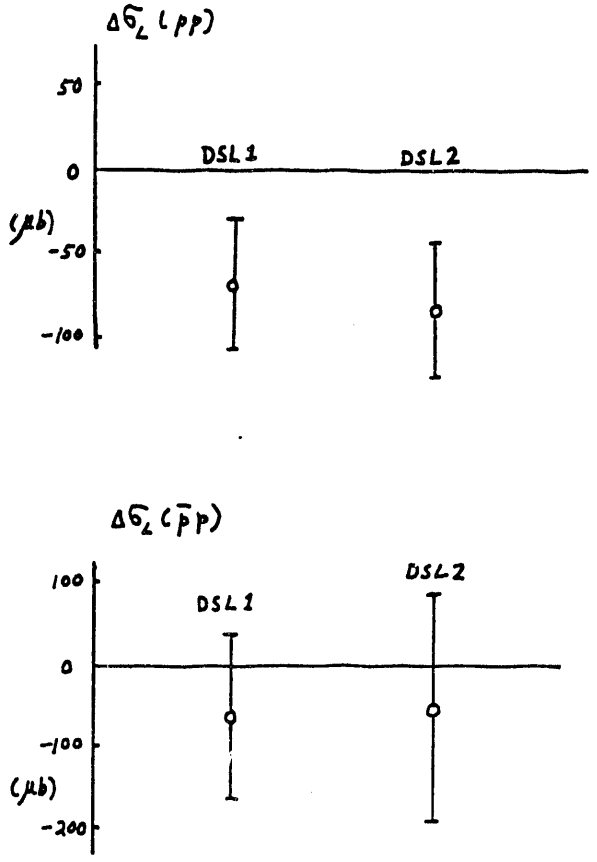

Figure 25. Preliminary data ("Saclay analysis", L. van Rossum et. al., private communication).

7. Study of the Spin-Dependent Parton Distribution with Polarized Protons

These studies can be made at Fermilab polarized-beam facility, planned polarized beams at UNK and proposed polarized collider at RHIC. In fact, the major motivation to construct the Fermilab polarized-beam facility was to obtain the gluon-spin information by measuring the asymmetry parameter A_{LL} for χ_2 and J/ψ production (proposal 675) and was many years before the "spin crisis".

7.1 Measurements of Parton Helicity Distribution in a Polarized Proton

Let us consider the hadronic reaction, pp $\rightarrow$ (hadron or gauge boson) + X. When both initial protons are longitudinally polarized, we measure an observable A_{LL}. If one QCD subprocess is dominant:

$$A_{LL} \sim P_a P_b \hat{a}_{LL} \; (a + b \rightarrow c + x), \text{ where}$$

P_a and P_b are polarization of partons a and b, respectively.

7.1.1 Gluon Helicity Distribution

i) $p^{\uparrow}p^{\uparrow} \rightarrow \chi_2 + X$

It is generally believed that the χ_2 (3555) state is mainly produced by gluon-gluon fusion. The observable A_{LL} is related to the distribution function of a polarized gluon in a polarized proton expressed as $G_+(x)$ and $G_-(x)$ with same- and opposite-sign helicities, respectively. The dependence is given by:

$$A_{LL}(x_F) = \left[\frac{\Delta G}{G}(x_1) \bullet \frac{\Delta G}{G}(x_2)\right] \hat{A}_{LL}$$

where x_1, x_2 are the longitudinal-momentum fraction of gluons, $x_F = x_1 - x_2$, $M^2_{\chi_2} = x_1 \cdot x_2 \cdot s$, $\Delta G/G(x) \equiv (G_+(x) - G_-(x)/(G_+(x) + G_-(x))$, A_{LL} is A_{LL} (χ_2) for two fully polarized gluons.

Fermilab 200-GeV/c polarized beam is in the unique energy region to investigate the gluon-spin distribution in the charmonium production. At collider energies, $M^2/s = x_1 \cdot x_2 \approx 0$. For a given x_F coverage, x_1 or x_2 is zero. So far, theoretical models predict $\Delta G/G(x) = 0$ at $x = 0$. Therefore, no information is obtained on $\Delta G/G(x)$ because A_{LL} is proportional to $\Delta G/G(x_1) \cdot \Delta G/G(x_2)$.

ii) Direct-γ Production

Direct photons are produced through the $q\bar{q}$ annihilation subprocess and the q-g Compton subprocess, $qg \rightarrow \gamma q$. The Compton process is the dominant one in pp interactions. Then,

$$A_{LL} = [\Delta u(x_1)/u(x_1)] \bullet [\Delta G(x_2)/G(x_2)] \bullet \hat{a}_{LL}(qg \rightarrow \gamma q),$$

where $\Delta u(x)/u(x) = [u_+(x) - u_-(x)]/[u_+(x) + u_-(x)]$ with $\Delta u(x)$ being the helicity distribution of the quark, and

$$\Delta G(x)/G(x) = [G_+(x) - G_-(x)]/[G_+(x) + G_-(x)] .$$

For example, $\Delta u(x)/u(x) \approx 0.4$ at $x_q = 0.2$ (from EMC-SMC), $\hat{a}_{LL} = 0.6$ at 90° scattering. Then we have $A_{LL} = 0.2 \times \Delta G/G$, and $\delta(\Delta G/G) = 5 \times \delta A_{LL}$.

For proper coverage of x region, a large $\sqrt{s}$ region is not a proper place.

iii) Jet Production

Several QCD subprocesses contribute to the cross section for jet production:

a) gluon-gluon scattering at low $p_\perp$,
b) gluon-quark scattering at medium $p_\perp$ (above ~ 20 GeV/c), and
c) quark-quark elastic scattering at high $p_\perp$.

At low $p_\perp$:

$$A_{LL} = [\Delta G(x_1)/G(x_1)] \times [\Delta G(x_2)/G(x_2)] \times \hat{a}_{LL}(gg \rightarrow gg)$$

The $\hat{a}_{LL}$ is expected to be large, $\hat{a}_{LL} = 0.8$ at 90°.

7.1.2 Sea-Quark Helicity Distribution

i) Drell-Yan Process

The Drell-Yan process appears to be one of the best ways to determine the polarization of sea quarks. The $q\bar{q}$ annihilation into a vector boson gives a large asymmetry at the partonic level, and selects sea antiquarks along with valence quarks.

The asymmetry A_{LL} for Drell-Yan in pp collisions is related to the sea-quark helicity distribution:

$$A_{LL} = \hat{a}_{LL} \frac{\sum_i e_i^2 \left[\Delta q_i(x_1)\Delta\bar{q}_i(x_2) + \Delta q_i(x_2)\Delta\bar{q}_i(x_1)\right]}{\sum_i e_i^2 \left[q_i(x_1)\bar{q}_i(x_2) + q_i(x_2)\bar{q}_i(x_1)\right]},$$

where $x_1 - x_2 = x_F$, $x_1 x_2 = M^2/s$, and $\hat{a}_{LL} = -1$.

ii) Parity-Violating Asymmetry in W and Z Production

W and Z production with polarized protons is a totally unexplored area. The predictions for asymmetries, in particular, for the parity nonconservation ones, are expected to be large.

The observable A_L^{PV} is defined as:

$$A_L^{PV} = \left(N^- - N^+\right) / \left(N^- + N^+\right).$$

W's are predicted to be produced by a parity-violating mechanism, using standard model couplings. For example, in the case of W^+ production:

$$A_L^{PV} = \frac{\Delta u(x_1)\,\bar{d}(x_2) - \Delta\bar{d}(x_1)\,u(x_2)}{u(x_1)\,\bar{d}(x_2) + \bar{d}(x_1)\,u(x_2)} \hat{a}_L$$

7.2 Measurements of Quark Transversity Distribution in Polarized Protons

We discuss measurements of $h_1(x)$ in the Drell-Yan process. From deep inelastic scattering, one can measure $f_1(x)$ related to the longitudinal momentum distribution of quarks in the nucleon and $g_1(x)$ related to the helicity distribution of a polarized nucleon. There exists a third fundamental function, $h_1(x)$, which is a leading-twist (twist-2) distribution function like $f_1(x)$ and $g_1(x)$. This can be determined by measuring the transverse spin asymmetry A_{NN} in Drell-Yan processes.

$$A_{NN} = \left(1/P^2\right)\left(N^{\uparrow\uparrow} - N^{\uparrow\downarrow}\right) / \left(N^{\uparrow\uparrow} + N^{\uparrow\downarrow}\right).$$

In terms of $h_1(x)$, A_{NN} is given as:

$$A_{NN} = \hat{a}_{NN} \frac{\Sigma_a e_a^2\, h_1^a(x_1)\, h_1^{\bar{a}}(x_2)}{\Sigma_a e_a^2\, f_1^a(x_1)\, f_1^{\bar{a}}(x_2)},$$

where $\hat{a}_{nn}$ is the partonic double-spin asymmetry.

7.3 One-Spin Measurement to Determine Spin-Dependent Quark-Gluon Correlation Functions

Single transverse spin asymmetries in hard processes are expected to vanish in pQCD. The asymmetries vanish at the leading-twist (twist-2) level, however, this is no longer true at twist-3.

A large asymmetry was predicted in $p^{\uparrow}p \rightarrow \gamma X$. (Experimentally, large A_N values were found in lower-energy experiments up to $p_T = 4$ GeV/c in $p^{\uparrow}p \rightarrow \pi^{\circ}X$).

The twist-3 parton distribution involves the correlation between quark and gluon field strength.

8. RHIC Polarized Collider and the STAR Detector

RHIC polarized collider and associated experiments will be covered by several colleagues. RHIC spin proposal, R5, contains experiments using detectors STAR and PHENIX. Here, I would like to describe how accurately measurements can be made within the acceptance of the STAR detector (see Fig. 26).

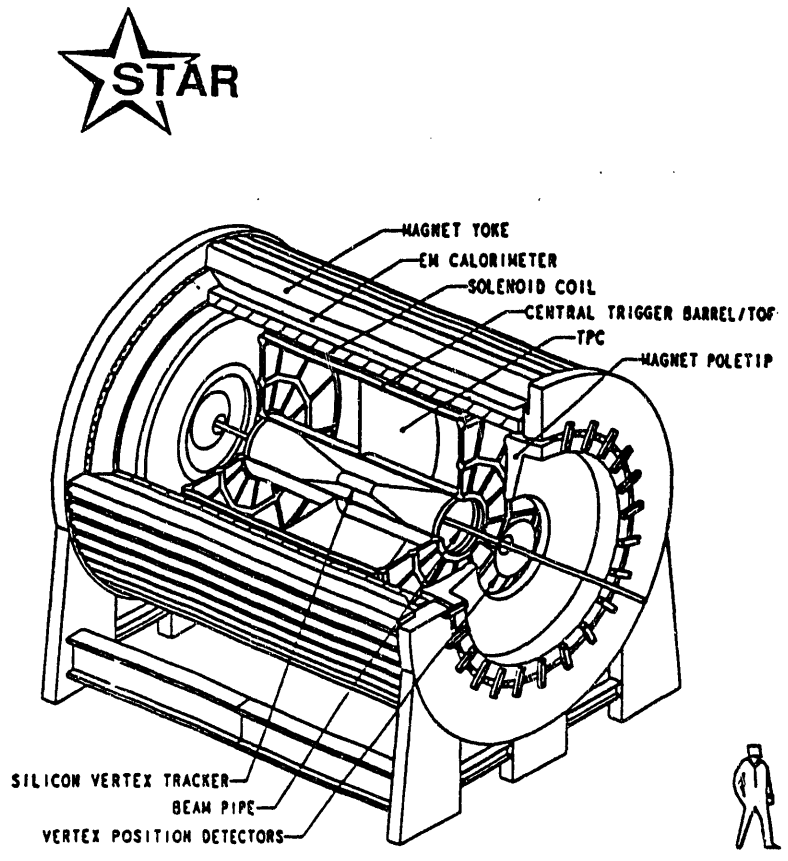

Figure 26. Perspective view of the STAR experimental configuration.

There are several areas of proton-proton spin physics that can be best done with a combination of RHIC and STAR. One of them is the gluon spin structure function with longitudinal spin in the proton. The gluon spin structure function, ΔG, can be determined crudely with inclusive jets, better with inclusive direct gammas, and best by using a direct gamma in coincidence with the production of an away-side jet and obtaining the x dependence of ΔG. The sea-quark polarization can be determined by measuring the longitudinal spin-spin asymmetries in the Drell-Yan process. The quark transversity distributions in a polarized proton have recently been discussed extensively by theorists and it is a fundamental measurement to determine the structure function $h_1(x)$. This can be done by measuring the transverse spin-spin asymmetries in the Drell-Yan process. Single-spin transverse asymmetries in π^0 production appear to remain constant at a given x_T up to 200-GeV/c. At the higher energies available at RHIC, it is unarguable that perturbative QCD should be fully applicable. Finally, the measurement of single-helicity asymmetries (parity violation) in $W^{\pm}$ and Z^0 production will be carried out.

We present the estimates of the acceptances of STAR and expected event rates for various reactions discussed earlier.

The integrated luminosities used are:

$$\int \mathcal{L}dt = 8 \cdot 10^{38}\ \text{cm}^{-2} \text{ at } 500\ \text{GeV} = 800\ \text{pb}^{-1},$$

and

$$\int \mathcal{L}dt = 3.2 \cdot 10^{38}\ \text{cm}^{-2} \text{ at } 200\ \text{GeV} = 320\ \text{pb}^{-1},$$

which means 100 days of running ($4 \cdot 10^6$ sec, 50% eff.).

8.1 Measurements with Barrel EM Calorimeter and Shower Maximum Detector

a) Direct-γ Production

With the assumed shower maximum 1-cm strips, the estimated δA_{LL} at $\sqrt{s}$ = 500 GeV is for p_T = 10 to 20 GeV, $\Delta y \pm 1$,

$$\delta A_{LL} \sim \pm (1/P^2)\ (0.0006 \sqrt{8 \times 10^{38}\ \text{cm}^{-2} / \int \mathcal{L}dt})$$

At $\sqrt{s}$ = 200 GeV,

$$\delta A_{LL} \sim \pm (1/P^2)\ (0.003 \sqrt{3.2 \times 10^{38}\ \text{cm}^{-2} / \int \mathcal{L}dt}).$$

b) Single-Jet Production

Jets can be detected in STAR and with the EM calorimeter for the EM component, and with the TPC for charged particles. Monte Carlo studies of the rates, acceptance, and resolution were made using the ISAJET program with EHLQ1 structure functions and GEANT.

Assume that particles within a core of radius $\sqrt{(\Delta\eta)^2 + (\Delta\phi)^2} = 0.7$ were part of the jet. Jet rapidity: $|\eta| < 0.3$, corresponding to $0.05 < x < 0.3$ at p_T = 10 GeV/c, $\sqrt{s}$ = 200 GeV.

c) Direct-γ + Jet

"γ + Jet" events with $-0.3 < \eta_{jet} < 0.3$ and $-1.0 < \eta_\gamma < 1.0$ determine the kinematics of the primary quark-gluon scattering.

For the p_T acceptance of 10 to 20 GeV, x_1 and x_2 vary from 0.1 to 0.2 at $\sqrt{s} = 200$ GeV. For the cross section in the p_T interval 15-20 GeV/c equal to 28 pb, the estimated uncertainty in A_{LL} is:

$$\delta A_{LL} \sim \pm (1/P^2)\,(0.017\sqrt{3.2 \times 10^{38}\ \mathrm{cm}^{-2}/\int \mathcal{L}dt}).$$

(remember $\delta(\Delta G/G) = 5 \times \delta A_{LL}$).

d) Di-Jet Production

The number of di-jet events, Npair at $\sqrt{s} = 200$ GeV (320 pb^{-1}) is given as:

Jet + Jet Events

M_{JJ}	$\lvert\eta\rvert$	N_{pair}
≥ 20	≤ 0.3	$3 \cdot 10^6$

e) One-Spin Measurement to Determine Spin-Dependent Quark-Gluon Correlation Function

The event rate for direct-gamma production can be estimated in a similar way as before,

$$\delta A_N \sim \pm \frac{1}{P}\,(0.004\sqrt{3.2 \times 10^{38}\ \mathrm{cm}^{-2}/\int \mathcal{L}dt}.$$

f) A_L^{PV} in W and Z Production

Production cross sections are estimated using PYTHIA v 5.3 for W and Z in pp interactions at $\sqrt{s} = 500$ GeV as

$$\sigma B(pp \rightarrow W^+ + X \rightarrow e^+ + \upsilon + X) = 120\ \mathrm{pb}$$
$$\sigma B(pp \rightarrow W^- + X \rightarrow e^- + \bar{\upsilon} + X) = 43\ \mathrm{pb}$$
$$\sigma B(pp \rightarrow Z^\circ + X \rightarrow e^+e^- + X) = 10\ \mathrm{pb}$$

The STAR detector with electromagnetic calorimeters is especially suitable for experiments with the W and Z due to its large acceptance for electrons produced by high mass particle decays.

The event rate estimates at $\sqrt{s} = 500$ GeV for the integrated luminosity 800 pb^{-1} are:

Boson	STAR (Barrel)
$W^+ + W^-$	83,000
W^+	61,000
W^-	22,000
Z°	3,840

8.2 Measurements with Endcaps

An important upgrade for the photon detection would be a pair of EM endcap calorimeters to be placed inside the iron pole piece as shown in Fig. 20. They would cover $|\eta| \leq 2.0$. Figure 21 shows the x coverage for $x_T = 2\,p_T/\sqrt{s} = 0.1$ as functions of the direct-γ and jet pseudorapidities, where x_1 and x_2 are given in terms of pseudorapidity as:

$$x_1 \simeq \frac{2p_T}{\sqrt{s}}\left(\frac{e^{\eta_1}+e^{\eta_2}}{2}\right),$$

and

$$x_2 \simeq \frac{2p_T}{\sqrt{s}}\left(\frac{e^{-\eta_1}+e^{-\eta_2}}{2}\right).$$

We summarize measurements and accuracy for various reactions discussed earlier.

a) Detecting with Direct-γ and the "Away-Side Jet (200 GeV)

δA_{LL}, Uncertainty in Asymmetry

	max (x_1, x_2)			
min (x_1, x_2)	≤ 0.2	0.2 - 0.3	0.3 - 0.4	> 0.4
0.00 - 0.05		0.012	0.009	0.007
0.05-0.10	0.006	0.006	0.010	0.012
0.10-0.15	0.007	0.010	0.020	0.030
0.15-0.20	0.021	0.019	0.038	0.060
> 0.20		0.035	0.049	0.073

b) Di-Jet Production (200 GeV)

p_T	$\|\eta\|$	N pair
≥ 20	≤ 1.3	$1 \cdot 10^8$

c) Sea-Quark Helicity Distribution (200 GeV)

M_{ee}, GeV/c^2	5-9	9-12	12-15	15-20
	28,000	20,000	8,400	5,400

d) $h_1(x)$ in the Drell-Yan Process (200 GeV)
26,000 events at mass region of 5 to 9 GeV ($\delta A_{NN} \approx \pm 5\%$ at $x_F = 0.20$)

e) W's and Z (500 GeV)

W+	80,000
W-	30,000
Z°	7,200

* Work supported by the U.S. Department of Energy, Division of High Energy Physics, Contract W-31-109-ENG-38.

References

1) A. Yokosawa, 1973, "Two-Body Final-State Hadronic Physics", ANL/HEP 7303, revised version of KEK-72-6 (1972).

2) A. Yokosawa, *Proc. 19th Int. Conf. High Energy Physics* (Tokyo, August 1978), A2, p. 39.

3) A. Yokosawa, 1980, *Phys. Reports* **64**, 47 and references therein.

4) A. Yokosawa, 1985, *Proc. 6th Int. Symp. Polar. Phenom. in Nucl. Phys.*, Osaka; 1986, J. Phys. Soc. Jpn., Suppl. **55**, 251, and references therein.

5) A. Yokosawa, 1990, *International Journal of Modern Physics A*, Vol. 5, No. 16, p. 3089, and references therein.

6) N. Hoshizaki et al., 1992, Nagoya Symposium.

7) R. L. Shypit et al., 1988, *Phys. Rev. Lett.*. **60**, 901; 1988, **61**, 2385; 1989, *Phys. Rev.* **C40**, 2203.

8) N. Hoshizaki, 1992, *Phys. Rev.* C45, R1424; N. Hoshizaki, 1992 Nagoya Symposium.

9) I. I. Strakovsky, May-June 1991, Fiz. Elem. Chastits At. Yadra **22**, 615.

10) R. J. Holt et al., 1979, *Phys. Rev. Lett.* **43**, 1229; R. J. Holt et al., 1981, *Phys. Rev. Lett.* **47**, 472; E. Ungrichhys, 1984, *Rev. Lett.* **52**, 333; E. Ungricht et al., 1985, *Phys. Rev.* **C31**, 934.

11) J. Ulbricht et al., 1982, *Phys. Rev. Lett.* **48**, 311; W. Gruebler et al., 1982,*Phys. Rev. Lett.* **49**, 444; V. Konig et al., 1983,*J. Phys.* **G9**, L211.

12) Y. M. Shin et al., 1985, *Phys. Rev. Lett.* **55**, 2672.

13) G. R. Smith et al., 1986, *Phys. Rev. Lett.* **57**, 803.

14) Y. Sumi and S. Uehara, 1986, *Prog. Theor. Phys.* **75**, 646.

15) K. Kanai et al., 1979,*Prog. Theor. Phys.* **62**, 153.

16) A. Rahbar et al., 1987, *Phys. Lett.* **B194**, 338.

17) C. Ohmori et al., 1989, *Phys. Lett.* **B230**, 27.

18) Sun Tsu-hsun et al., 1985, *Phys. Rev.* C31, 515.

19) G. Alberi et al., 1982, *Ann Phys.* (N.Y.) **142**, 299, and references therein.

20) G. Igo et al., 1988, *Phys. Rev.* C38, 2777.

21) D. L. Adams et al., 1988, *Nucl. Phys.* **A480**, 530.

22) G. Igo et al., 1988, *Proc. 8th Int. Symp. on High Energy Spin Physics*, Minnesota, ed. K. J. Heller, AIP Conf. Proc. No. 187, Vol. I, p. 668.

23) I. I. Strakovsky, A. V. Kratsov, and M. G. Ryskin, 1984,*Yad. Fiz.* **40** (1984) 429 (*Sov. J. Nucl. Phys.* **40**, 273).

24) E. Aprile-Giboni et al., 1984, *Nucl. Phys.* **A431**, 637.

25) A. B. Wicklund et al., 1987, *Phys. Rev.* **D35**, 2670.

26) N. Tanaka et al., 1988, *Phys. Rev.* **C37**, 2071.

27) N. R. Stevenson and Y. M. Shin, 1987, *Phys. Rev.* **C36**, 1221.

28) R. A. Arndt et al., 1987, *Phys. Rev.* **D35**, 128.

29) N. Hiroshige, W. Watari, and M. Yonezawa, 1984, *Prog. Theor. Phys.* **72**, 1287.

30) D. V. Bugg, 1984, *J. Phys.* **G10**, 717.

31) G. Glass et al., 1985, *Phys. Rev.* **C31**, 288.

32) D. B. Barlow et al., 1988, *Phys. Rev.* **C37**, 1977.

33) T. Mizutani et al., 1981, *Phys. Lett.* **B107**, 177, and references therein.

34) A. Saha et al., 1983, *Phys. Rev. Lett.*. **51**, 759; K. K. Seth et al., 1983, Phys. Lett. **B126**, 164.

35) R. Bertini et al., 1985, *Phys. Lett.* **B162**, 77; 1988, *Phys. Lett.* **B203**, 18.

36) See review by B. Tatischeff, 1985, *Nucl. Phys.* **A446**, 355.

37) B. Tatischeff et al., 1984, *Phys. Rev. Lett.* **52**, 2022; 1987, *Europhys. Lett.* **4**, 671; 1987, *Z. Phys.* **A328**, 147; 1987, *Phys. Rev.* **C36**, 1995.

38) L. Santi et al., 1988, *Phys. Rev.* **C38** (RC), 2466.

39) M. H. MacGregor, 1979, *Phys. Rev. Lett.* **42**, 1724.

40) P. J. G. Mulders et al., 1980, *Phys. Rev.* **D21**, 2653.

41) N. Willis et al., 1989, *Phys. Lett.* **B229**, 33.

42) T. Ueda, 1991, *Phys. Rev. Lett.* **66**, 297; Nagoya Conference.

43) D. G. Crabb et al., 1990, *Phys. Rev. Lett.* **65**, 3241.

44) T. deGrand and H. I. Miettinen, 1981, *Phys. Rev.* **D24**, 2419; 1985 *Phys. Rev.* **D31** (E), 661, and references therein.

45) B. Anderson et al., 1983, *Phys. Rep.* **97**, 31, and references therein.

46) J. Szwed, 1981, *Phys. Lett.* **105B**, 403.

47) P. G. Ratcliffe, 1985, *Proc. 6th Int. Symp. on High Energy Spin Physics*, Marseille, ed. J. Soffer, Journal de Physique **46**, C2, p. 31.

48) A. B. Efremov and O. V. Terjaev, 1987, *Proc. 7th Int. Symp. on High Energy Spin Physics*, Protvino, USSR, IHEP, Serpukhov, Vol. I, p. 89.

49) M. Sullivan et al., 1984, *Phys. Lett.* **142B**, 451; 1987, *Phys. Rev.* **D36**, 674.

50) E. C. Dukes et al., 1987, *Phys. Lett.* **193B**, 135.

51) B. E. Bonner et al., 1989, *Phys. Rev. Lett.* **62**, 1591.

52) P. M. Ho et al., 1990, *Phys. Rev. Lett.* **65**, 1713, and references therein.

53) H. T. Diehl et al., 1991, *Phys. Rev. Lett.* **67**, 804 and references therein.

54) H. J. Lipkin, 1985, *Nucl. Phys.* **B214**, 136; L. Brekke and J. L. Rosner, 1988, *Comments Nucl. Part. Phys.* **18**, 83.

55) J. Duryea et al., 1991, *Phys. Rev. Lett.* **67**, 1193.

56) D. Grosnick et al., 1990, *Nucl. Instrum. and Meth.* **A290**, 269.

57) D. C. Carey et al., 1990, *Phys. Rev. Lett.* **64**, 357.

58) J. Schwinger, 1948, *Phys. Rev.* **73**, 407.

59) For instance, C. Bourrely and J. Soffer, 1977, *Nuovo Cimento Lett.* **19**, 569.

60) N. Akchurin et al., 1989, Phys. Lett. **B229**, 299.

61) B. Z. Kopeliovich and L. I. Lapidus, 1974, Yad. Fig. 19, 218; 1974, *Sov. J. Nucl. Phys.* 19, 114.

62) N. H. Buttimore, E. Gotsman , and Am. E. Leader, 1978, *Phys. Rev.* **D18**, 694.

63) N. H. Buttimore, 1985, *Proc. 6th Int. Symp. on High Energy Spin Physics,* Marseille, Ed. J. Soffer, Journal de Physique, **46**, C2, 643.

64) N. Akchurin et al., to be published.

65) D. L. Adams et al., 1992, *Phys. Lett.*, **B276**, 531.

66) S. Sanoff et al., 1990, *Phys. Rev. Lett.* **64**, 995.

67) J. Antille et al., 1980, *Phys. Lett.* **B94**, 523.

68) V. D. Apokin et al., 1990, *Phys. Lett.* **B243**, 461.

69) D. L. Adams et al., 1991, *Phys. Lett.* **B261**, 201.

70) B. E. Bonner et al., 1988, *Phys. Rev. Lett.* **61**, 1918.

71) J. Soffer and N. A. Tornquist, 1992, Phys. Rev. Lett. **68**, 907.

72) T. deGrand and H. I. Miettinen, 1981, *Phys. Rev.* **D24**, 2419; 1985, *Phys. Rev.* **D31** (E) 661.

73) D. L. Adams et al., 1991, *Phys. Lett.* **B264**, 462.

74) J. Soffer and D. Wray, Wis-72/31-ph, unpublished.

75) E-704 preliminary data.

76) P. Kroll, 1990, *University of Wuppertal Report* No. WU B 90-17.

77) D. Sivers, 1990, *Phys. Rev.* **D41**, 83.

78) Meng Ta-chung et al., 1989, *Phys. Rev.* **D40**, 769; Liang Zuo-tang and Meng Ta-chung, 1990, *Phys. Rev.* **D42**, 2380; Liang Zuo-tang and Meng Ta-chung, 1991, Institut für Theoretische Physik der Freien Universität Berlin Report No. FUB-HEP/91-8, to be published.

79) J. Qiu and G. Sterman, 1991, *Phys. Rev. Lett.* **67**, 2264.

80) P. Chaumette et al., 1990, *Proc. 9th Int. Symp. on High Energy Spin Phys.*, Bonn, Germany, p. 237.

81) D. L. Adams et al., 1991, *Phys. Lett.* **B261**, 197.

82) G. Ramsey and D. Sivers, 1990, *Argonne Internal Report ANL-HEP-PR-90-76.*

END

DATE
FILMED
3/23/93